The Effect of Elevation on Single Event Upsets in Digital Imagers

by

Simone Neufeld

Undergraduate Thesis Submitted in Partial Fulfillment of the

Requirements for the Degree of

Bachelor of Applied Science

in the

School of Engineering Science

Faculty of Applied Science

© Simone Neufeld 2021

SIMON FRASER UNIVERSITY

Fall 2021

Approval

Name: Simone Neufeld

Degree: Bachelor of Applied Science

Title of Thesis: The Effect of Elevation on Single Event Upsets in Digital Imagers

_____

Michael Sjoerdsma
Acting Director, School of Engineering Science

Examining Committee:

**Academic and
Technical Supervisor:**

_____

Dr. Glenn H. Chapman, P. Eng.
Director, School of Engineering Science

Committee Member:

_____

Dr. Marinko V. Sarunic, P. Eng.
Professor, School of Engineering Science

Committee Member:

_____

Dr. Michael Adachi, P. Eng.
Professor, School of Engineering Science

Dec 15. 2021

Date Approved: _____

Abstract

Cosmic radiation causes transient errors in microelectronic devices, known as Single Event Upsets (SEUs). These errors are most common in space-borne electronics, however terrestrial electronics experience the same errors, to a lesser degree. SEUs can be difficult to characterize in most integrated circuits, however, in digital imagers they cause defects which appear as unexpected bright pixels that are temporarily present in a series of images. To detect them, a sequence of long exposure, dark-frame images is recorded and then during analysis pixels which appear bright in one photograph but dark in the images immediately before and after are flagged. Just as the effect of SEUs is more prevalent in space, a rise in elevation on Earth can increase the frequency of SEUs by a noticeable amount. In this thesis, I will perform a series of experiments to understand the relationship between SEUs and elevation. Using DSLR cameras, images will be recorded at elevations ranging from sea level to approximately 1200 metres above sea level. The quantity and charge distribution of the SEUs will be extracted from the photographs and compared to the elevation.

Keywords: Single event upsets; elevation; digital imager defects; cosmic radiation

Acknowledgements

     I would like to thank my committee members Dr. Glenn Chapman, Dr. Marinko Sarunic, and Dr. Michael Adachi for their guidance on my thesis as well as their support during the entirety of my degree. A special thanks to Dr. Glenn Chapman for offering his time and feedback over the past year, I would not have been able to complete this project without his knowledge and experience.

     A special thank you to my friends Arvin Amini and Sophia Phillips for their assistance with collecting data for my research. Their time and patience were greatly appreciated.

     Lastly, I want to thank my parents, sister, and grandmothers for their continual support during my degree. I would not have been able to come this far without the support of my family.

Table of Contents

List of Tables

List of Figures

Chapter 1.

Introduction

1.1. An Abridged History of Cameras

Cameras, invented nearly two centuries ago, date back to the first photograph taken in 1826 by the French inventor Nicéphore Niépce. Prior to this, the camera obscura phenomenon, was discovered thousands of years before, although not a true camera, since the image was not recorded, simply projected onto a surface. Originally documented around 500 BCE, by Chinese philosopher Mo Ti, the camera obscura phenomenon occurs when light enters a dark chamber through a pinhole and projects an inverted image of the scene outside the chamber onto the wall opposite the hole. This concept was frequently used by artists in the 16th and 17th century to aid in drawing perspective, and the phenomenon is essentially how modern-day cameras function. While the camera obscura projects light onto a surface, that image must also be recorded somehow. Prior to the invention of film cameras, and even before Niépce developed a process to take photographs, the English inventor Thomas Wedgwood experimented with exposing silver nitrate to light to create an image in the 1790s. He was able to create images, however he lacked a fixative to prevent the silver nitrate from further developing when exposed to light, because of this his images were only temporary. Once film cameras were developed, the film would be exposed to record an image via a chemical reaction, conversely with digital cameras, a sensor electronically records the levels of light [1].

The first permanent photograph was made by Niépce sometime in the 1820s, on a pewter plate with light sensitive asphalt, and had an exposure time of eight hours. Sunlight was used to cure the liquid asphalt so the unexposed portions on plate could be etched, creating a negative of the image. Shortly after Niépce's first photograph, he briefly worked with an artist named Louis Daguerre, who went on to develop the daguerreotype, the first photographic process on the market, in 1839. The daguerreotype process used a copper plate coated in silver halide to capture an image. Photographic film to this day still contains silver halide crystals, using their light sensitive properties to capture photographs. Nearly 40 years later, after much progress in photography, the first camera to use rolls of plastic film coated with silver halide came on the market in 1888, called the "Kodak".

Compared to today's cameras, it was very rudimentary, with a single shutter speed and a fixed-focus lens. The Kodak came preloaded with enough film for 100 pictures, when you finished a roll of film you mailed the camera back to the manufacturer and they developed your photos, added a new roll of film to the camera and sent it back to you [1].

Over the next century many developments were made in film cameras. They became smaller, cheaper, and had more features, such as adjustable focus, different shutter speeds, and different types of film, including readily available colour film, which included the trade-off of having a much more complex development process. Notable drawbacks of film cameras are the time needed to develop photos and the cost per photo. Until instant Polaroid cameras were released in 1948, users had to wait hours of even days for their photographs to be developed. Additionally, if you compare the costs of film and digital photography it is undeniable that digital is cheaper per photo. Ignoring the initial cost of a camera, film costs approximately 50 cents per photo while an SD card can store tens of thousands of photos for approximately 0.02 cents per photo. In the 1970s digital cameras were just starting to be developed, beginning with Charge-Coupled Device (CCD) sensors and later Complimentary Metal-Oxide-Semiconductor (CMOS) sensors. Nowadays, nearly all modern cameras contain CMOS sensors, while CCD cameras and film cameras become increasingly uncommon, only being used for specialized applications [1], [2].

1.2. Cosmic Rays Causing Soft Errors

Around the same time as cameras were being developed, the study of cosmic rays was beginning. Radioactivity was first discovered by Henri Becquerel in 1896, when it was detected in uranium. Later, a number of scientists, despite the assumption that radiation was solely emitted from the Earth, discovered that in fact, radiation increased with increases in altitude. In 1900, Julius Elster and Hans Geitel conducted experiments to measure radiation at sea level compared to in the Swiss Alps and noted a rise in radiation as the elevation rose, however scientists still believed the radiation was of terrestrial origin [3], [4]. It was only later in 1912, when Austrian physicist Victor Hess was conducting experiments on radiation from a hot air balloon. He noticed that radiation in fact increased significantly as elevation increased. One of his many hot air balloon trips was also taken

during a solar eclipse, Hess noted that during the eclipse the radiation was constant, and concluded it was not of solar origin. Later, a physicist named Robert Millikan continued Hess' research, eventually proving this radiation was of cosmic origin, and coined the term "cosmic rays" [3].

In fact, cosmic rays are not really rays, but rather particles originating in outer space, that can reach Earth and cause disruptions in electronics. Cosmic rays can be grouped into four types: primary cosmic rays, solar cosmic rays, secondary cosmic rays, and terrestrial cosmic rays. Originating outside the solar system, likely formed by stellar flares and supernovae, primary cosmic rays have lifetimes of approximately 200 million years and extremely high energies. As the name suggests, solar cosmic rays are outputted by the sun and do not have as high an energy as primary cosmic rays, meaning they only reach Earth during the active period of the sun's 11-year cycle. When primary cosmic rays in Earth's atmosphere collide with atmospheric nuclei, they create cascades of secondary particles. Any cosmic rays which manage to reach Earth are labelled as terrestrial cosmic rays, with less than 1% of these being primary cosmic rays. Cosmic rays are generally neutrons, protons, heavy ions, pions, and muons, with muons being the most abundant at sea level. However, muons are not the main cause of errors in electronics, but rather protons and neutrons are [5], [6].

As mentioned before, the sun operates on an 11-year cycle, with 7 of those years being an "active period" and the remaining 4 years being a "quiet period" [7]. During the quiet period, most solar cosmic rays do not have enough energy to reach Earth, however during the active period, the number of solar cosmic rays increases by a million times, causing a significant amount to reach sea level on Earth. Simultaneously, during the active sun period the magnetic field around Earth increases, due to an uptake in solar wind. This change in magnetic field blocks galactic cosmic rays from reaching Earth and reduces terrestrial cosmic rays. Additionally, the effect of the changing solar cycle is only experienced on Earth approximately two years after the change. Currently, the sun is experiencing a quiet period, where the trend of solar cycles is shown in Figure 1.1. Surprisingly, an increase in terrestrial cosmic rays will in fact be experienced during the quiet period of the sun due to the decrease in the magnetic field from solar wind being a more significant factor than the increase of solar cosmic rays during the active period [5], [7].
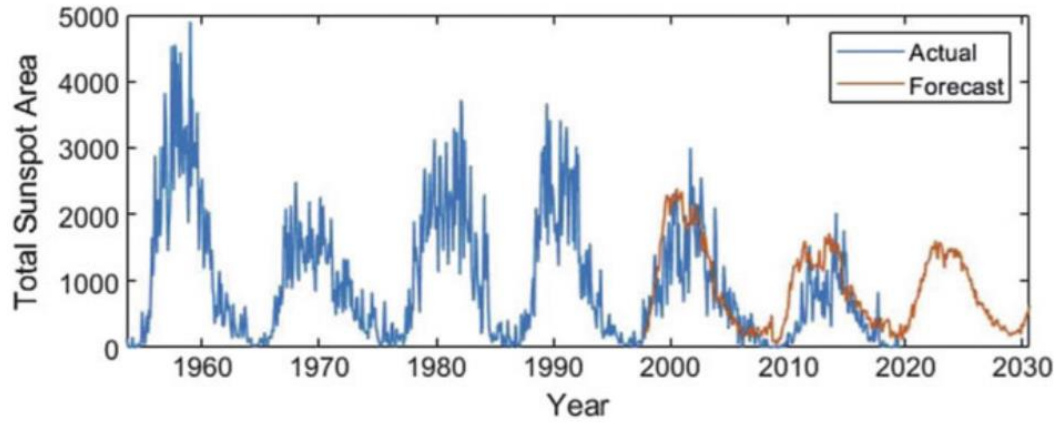
Figure 1.1: Total Sunspot Area from 1960 to 2030. Source: Taken from [8]

`

The magnetic field around Earth is not spherically symmetric, notice in Figure 1.2 the magnetic field lines are very different towards Earth's poles than towards the equator. This in fact causes the behaviour of cosmic rays to change depending on latitude, with locations towards the North and South poles experiencing greater occurrence rates of cosmic rays [7].
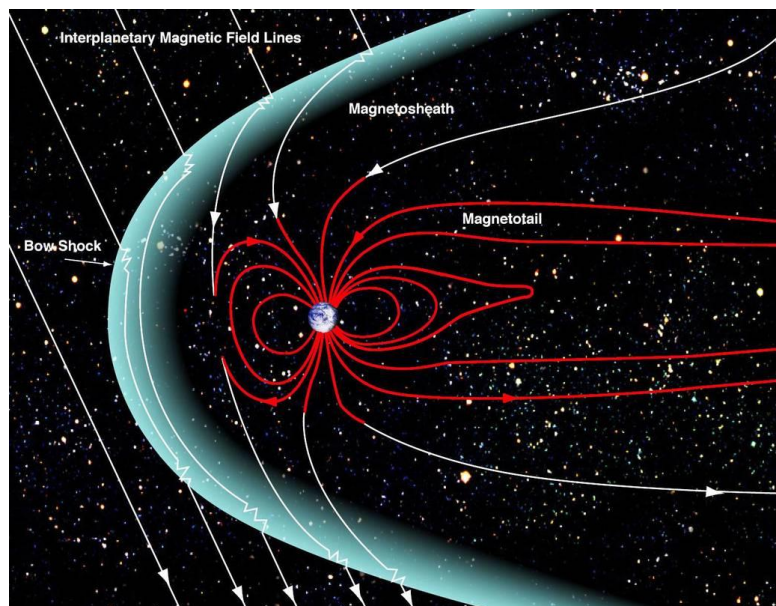
Figure 1.2: Earth's Magnetosphere. Source: Taken from [9]

Magnetic rigidity is a measure of how easily a cosmic ray can cross magnetic field lines, with more energetic (higher magnetic rigidity) particles being able to cross magnetic field lines more readily [10]. To reach the surface of Earth, the magnetic rigidity of the particle must be high enough, with it requiring a much lower magnetic rigidity for a particle to reach Earth near the poles than it is to reach the equator. To complicate matters even more, cosmic rays do not travel in straight lines, the computed trajectory for a cosmic ray that has high enough magnetic rigidity to reach Earth is shown in Figure 1.3.
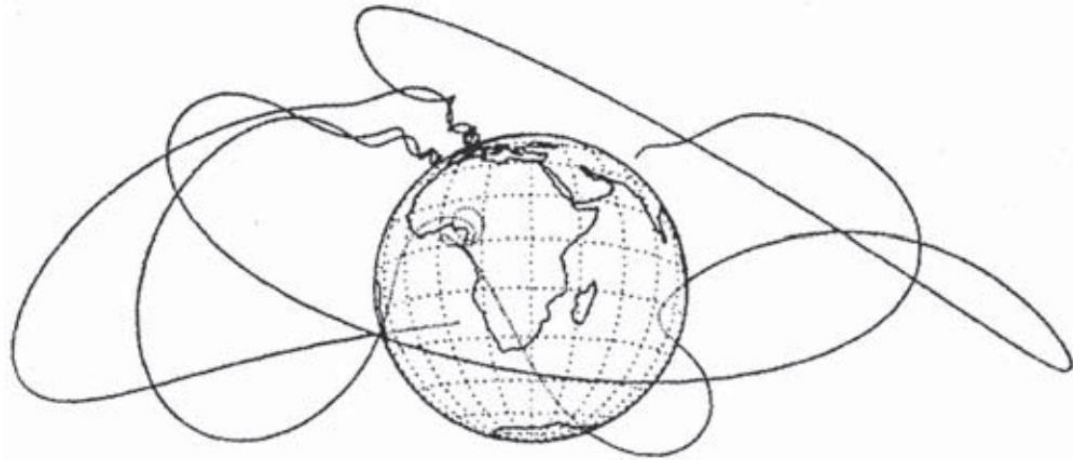
Figure 1.3: Computed Cosmic Ray Trajectory within Earth's Magnetic Field. Source: Taken From [10]

The effects of cosmic rays on electronics, called single event effects, were originally documented in 1962 by Wallmark and Marcus [7]. They cited it as being the "most severe limitation" on the packing density of semiconductor devices. Due to the relatively large size of conventional electronic components, and the rarity of cosmic rays, disturbances in conventional electronics are less common. Wallmark and Marcus also stated that cosmic radiation increases towards the North and South poles, or with an increase in elevation [7] Table 1.1 demonstrates how early research has found a link between the rates of cosmic rates and changes in elevation. You can see that on average for each 1500-metre increase in elevation, the rate of events doubles. The rates are higher at latitudes more than 40° above the equator, since Earth's magnetic field is better at rejecting incident particles near the equator [10]. For reference, Vancouver, BC is at approximately 50° North of the equator.

5

Table 1.1: Rates of Cosmic Rays at Different Altitudes and Latitudes. Source: Adapted from [7]

Altitude [m]	Dose Rate at Equator [mrads/year]	Dose Rate at Latitudes Greater than 40° [mrads/year]
Sea Level	23	26
1500	28	42
3000	56	84
4500	110	170

Single Event Effects (SEEs), defined as an observable change in state of a microelectronic component due to being struck by a cosmic ray [11], can be categorized into hard and soft errors, or rather permanent and temporary errors. Single event upsets (SEUs) are a type of soft error and can be further categorized into single bit upsets and multiple bit upsets [11]. Single bit upsets in digital photographs manifest as a single bright pixel, while multiple bit upsets appear as a streak or cluster of bright pixels.
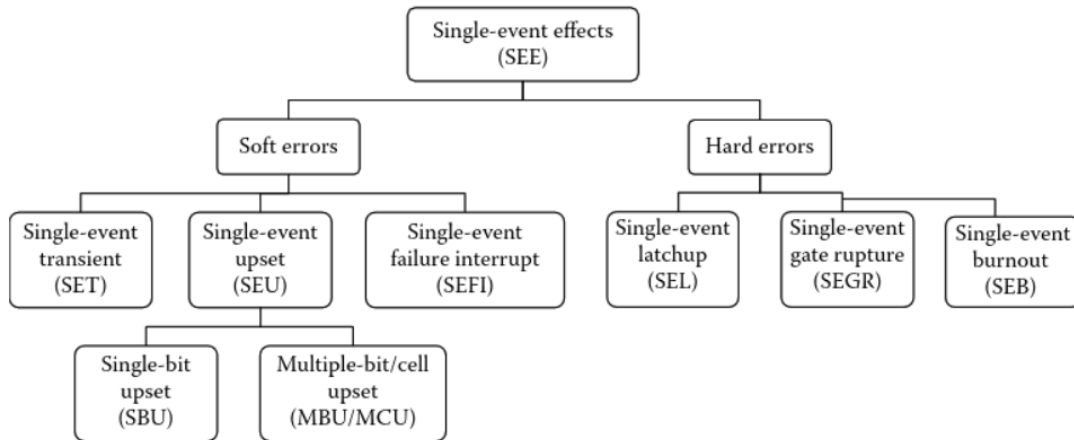
Figure 1.4: Categorization of Single Event Effects. Source: Taken from [11]

An example of an SEU streak is shown below in Figure 1.5. While this image is zoomed in very close, you can see that multiple pixels are affected by the SEU.
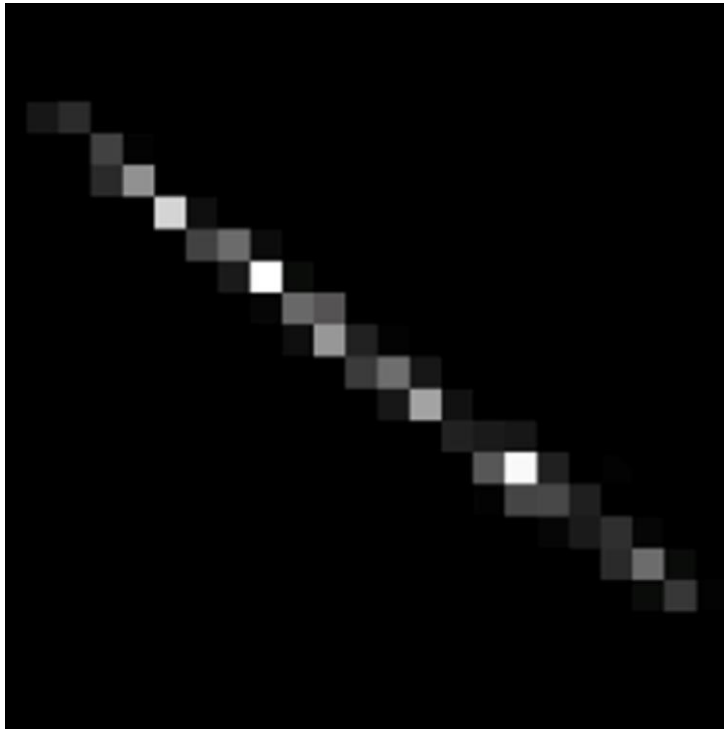
Figure 1.5: Example of an SEU Streak Recorded in a Digital Camera. Taken from [12]

Now, you cannot simply classify any bright pixel, or group of bright pixels as an SEU. The key criteria it must meet includes being transient, meaning if you use the same imager to record multiple photographs, a given bright pixel (or cluster) should only appear in that spot in a single image, and not in the images before and after. Detecting SEUs in photos will be explained in more detail in section 2.3.1.

On the contrary, hot pixels are another type of defect in photography caused by cosmic rays. They are not transient, meaning they are classified as a hard error, and they develop over time. A hot pixel will appear as a single bright pixel in an image, and in a series of images it will stay in the same location in every picture, however the brightness can change if there is more, or less, incident light, or if the camera settings are changed. The key difference between SEUs and hot pixels is that hot pixels occur in a fixed location set by the cosmic ray strike, while SEUs appear at random. Another type of hard defect is a stuck pixel, which will stay at the same intensity no matter the incident light. Stuck pixels are generally a manufacturing defect and should not get significantly worse over time.

Camera manufacturers are also able to manually mask any stuck pixels when calibrating a camera to remove them.

Hot pixels are caused by cosmic rays of high charge hitting the camera's sensor and permanently damaging a pixel. Over time the number of defects from hot pixels will increase and is dependent on pixel size, with hot pixels occurring more rapidly in cameras with smaller pixels sizes. Additionally, the altitude of a camera can affect the rate at which hot pixels are formed, due to the increase in cosmic rays at high elevations, a given camera will experience more hot pixels than if it were kept at a lower elevation [13]. When a camera is new, there should be minimal hot pixels, but after prolonged use, they will build up and become more noticeable. Both hot pixels and stuck pixels are different from single event upsets, and therefore will not be discussed in detail.

1.2.1. SEU Detection in Traditional ICs

Due to the transient nature of SEUs, they are not a common concern in photography and are often simply regarded as noise in photos. However, they can become a major concern in other types of electronics in high radiation environments, such as space where they create false results [14]. Alternative approaches to detect SEU effects often include exposing electronics to an irradiated environment to induce SEUs [15], [16] or simulating an SEU by artificially injecting an error [14]. When designing a system to test for SEUs there is a trade-off between the controllability and observability of the procedure and the cost and intrusiveness of the system[14]. When a cosmic ray passes through a semiconductor device electron-hole pairs are created, causing a logic bit to change state which can then propagate through the device [17], [18]. In previous research, SEUs have been investigated in CCD imagers [6], [15], [16] however this thesis will focus on CMOS imagers. A common detection method for errors caused by SEUs is to run multiple identical programs simultaneously and flag any instances where the outputs are not identical [14]. This method can be used for the purposed of studying SEUs but also for the purpose of correcting them in electronics where errors are detrimental.

1.3. Summary

With DSLR cameras being readily available, they make a perfect apparatus to record SEUs since the location and time of the SEU is recorded with the camera, unlike in a traditional IC where the defect would be difficult to locate. In this thesis three different cameras will be taken to a variety of modest elevations, ranging from sea level to approximately 1200 metres above sea level. The following chapters will discuss what results are drawn from this. Chapter 2 will introduce any background knowledge required to understand the following chapters. Chapter 3 will explain the procedure used to carry out experiments and the detection methods for SEUs. In Chapter 4 the results of the SEU detection algorithm will be presented and explained. Here data for the various cameras at different ISOs and elevations will be plotted. Finally, Chapter 5 will summarize the results and list any recommendations for areas of future research.

Chapter 2.

Digital Cameras and Single Event Upsets

2.1. Digital Camera Settings

DSLR cameras have a range of settings the user can manipulate when taking a photograph to get the best result. The most basic of these settings are ISO, exposure time, and aperture, all of which originated in film photography and control the amount of light entering the camera in different ways.

2.1.1. ISO

Dating back to film photography, ISO originally was a property inherent to the film a photographer used. Essentially, ISO is the sensitivity of the film, with slow films, or lower ISOs, being less sensitive to light, and fast films, or higher ISOs being more sensitive. Generally, lower values of ISO are used when the photographer is in bright light, such as outside on a sunny day. Higher ISOs are used for photographing a darker scene such as indoors or at night. In film photography, once film with a specific ISO is loaded into the camera, the ISO cannot be changed until that roll of film is finished and a new roll is inserted. However, the beauty of digital photography is that the photographer can change the ISO at any point, additionally, digital photography has a much larger range for ISOs than film provides.

ISOs typically start at 100 and double each time you increase the value. For photography, ISO 100 would be a good level to use in direct sunlight for a camera with an exposure time set to 1/60 seconds. For film photography the most common ISOs are 100, 200, 400, and 800, while for modern DSLRs they typically range from 100 to 12800, or even higher. When ISO is doubled, the sensitivity of the film, or the gain of the pixels in an image is doubled, meaning the higher the ISO the brighter the image will appear. Higher ISOs can be used when shooting a darker scene to give a brighter image. If ISO is increased too much, a scene can become overexposed, meaning some of the film or pixels are saturated and cease to record how the scene truly looked. In Figure 2.1(a) you can

see some details in the sky that are completely obliterated when the ISO is increased in Figure 2.1(b).
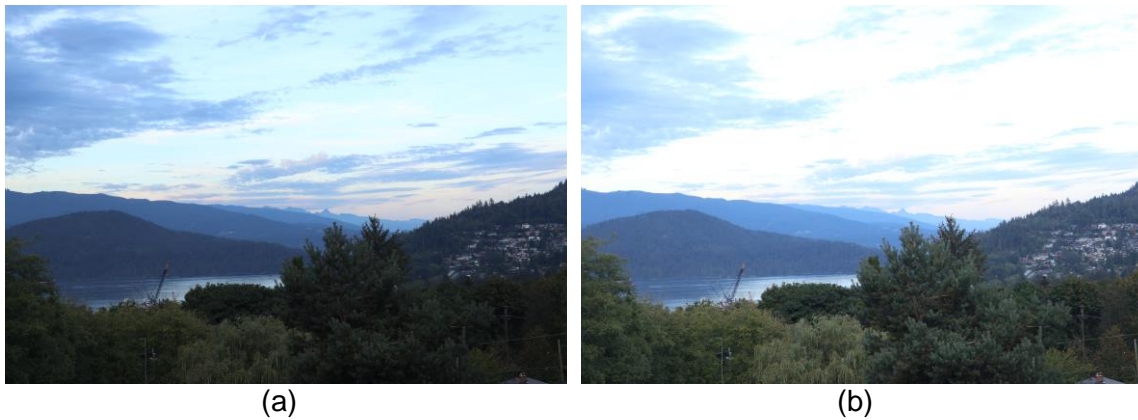
Figure 2.1: Comparison of Doubling ISO for Photos Taken at (a) ISO 200 and (b) ISO 400.

Additionally, when ISO is increased, images tend to look more "grainy". In film photography this is due to the physical size of grains of silver halide in the film. High ISO film has larger grains and low ISO film has smaller grains, causing higher ISO film to have lower resolution. Similarly in digital photography, higher ISOs lead to lower resolution, but it is for an entirely different reason. In digital photography any noise from the sensor will also be amplified, along with the image, causing photographs at higher ISOs to look noisy. To reduce noise, noise suppression algorithms are built into digital cameras, and they trade off resolution against noise. However, the noise suppression algorithms do not eliminate all the noise.

2.1.2. Exposure Time

In photography, exposure time also controls how much light is let into the camera in a different way. Simply put, exposure time is how long the shutter is open for, in film photography this would be how long the film is exposed to the light, while in digital photography it is how long the digital sensor is exposed to light. Exposure time is controlled with a setting called shutter speed, but the terms "exposure time" and "shutter speed" can be used interchangeably when referring to how long the shutter is open for.

Typical speeds range from a fraction of a second up to 30 seconds. Again, each time you increase exposure time, the value doubles generally, although there are some

exceptions, such as when you go from 1/125 seconds to 1/60 seconds or when you go from 8 seconds to 15 seconds. You can also set the shutter speed to any duration between these steps as well. Cameras can also have a shutter speed called "bulb" which allows for any duration of shutter speed. Essentially, the shutter will remain open for as long as the user is holding the shutter release down, this allows for exposures longer than 30 seconds.

The longer the shutter is open for, the more light is let in, and the brighter the image. If the exposure time is too fast then the image will be underexposed and appear too dark, contrastingly, if the exposure time is too slow the image will become overexposed and will be too bright. Additionally, if the shutter speed is too long it can cause motion blur, which is when the subject moves during the photograph or if the camera is not stable enough for long exposures. In certain types of photography motion blur can be used as a technique to show movement, however usually it is undesirable. Figure 2.2 shows an example of doubling exposure time while keeping all other factors constant. In Figure 2.2(a) you can see that the trees at the bottom of the picture appear dark and the details are hard too see, while in Figure 2.2(c) the trees show structure but the details in the sky are completely washed out and appear totally white, this is an example of what happens when an image is over or underexposed.

| (a) | (b) | (c) |
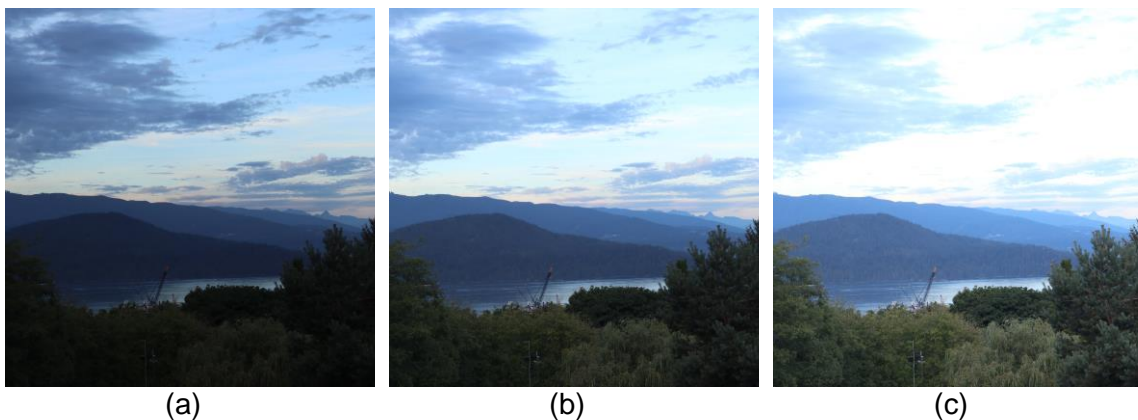
Figure 2.2: Comparison of Doubling Exposure Time for Photos with an Exposure Time of (a) 1/30 seconds, (b) 1/15 seconds, and (c) 1/8 seconds.

When exposure time increases, noise levels also increase proportionally. For any exposures longer than 30 seconds, the photographer is often limited by the amount of noise building up. There are methods available to mitigate noise, such as dark frame

subtraction, which will be explained in section 3.2, however this has drawbacks since any photo will take twice as long to be recorded, since two photos must be taken at the same exposure time. Additionally, the camera does have built-in algorithms to reduce noise, however these are proprietary and photographers have no control over them.

Generally long exposures are used for certain types of photography, such as landscape photography or astrophotography. In landscape photography, long exposures can be used as a tool to capture movement, often showing the movement of bodies of water. In astrophotography, long exposures are used due to the dim lighting conditions.

2.1.3. Aperture

Aperture refers to how large or small the opening letting light into the camera is. A small f-number corresponds to a large opening while a large f-number corresponds to a small opening. F-numbers typically range from f/2.8 to f/22, where the values increase by √2 each time. Aperture also controls how much of the scene will be in focus, with a large aperture (small f-number) having a small depth of field, and a small aperture (large f-number) having a large depth of field, meaning the entire scene will be in focus. Figure 2.3 below shows an example of how decreasing the f-number lets more light into the camera and brightens the scene.

(a)　　　　　　　　　　　　　　　　(b)
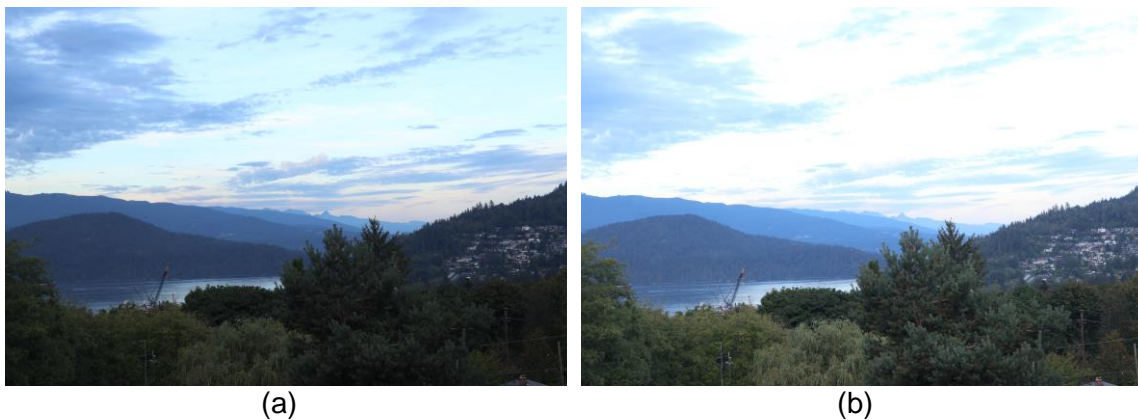
Figure 2.3: Comparison of Changing the f-number by one f-stop Photos with (a) f/16 and (b) f/11.

2.1.4. Image Format

When using a DSLR to record images, the photographer can generally decide whether they want images saved as JPEGs, RAW images, or both. For traditional photography, RAW images will require post-processing, such as in Photoshop, and then will be saved as another file format, such as JPEG. For our purposes, the photos were only recorded using Canon's RAW format, called "Canon Raw 2" or "CR2", and then converted to TIFF files.

When a photograph is taken with a digital camera, once the CMOS sensor is finished gathering data and the shutter is closed, a RAW image is generated, this image may include some initial noise suppression, but records each pixel output and does not include any compression or demosaicing. Next, a compressed JPEG image will be constructed from the RAW format, this JPEG image will have demosaicing and noise suppression applied, and the image will be compressed.

JPEG files are the smallest of the three types mentioned, and the most common. They produce a lossy image, meaning that the compression is irreversible, which is not ideal for editing, but the files are relatively small and do not require any post-processing. While JPEG involves an irreversible compression algorithm, since some of the data is discarded, there is a trade off between quality of the image and the size of the file. Digital RAW images are lossless and display data directly from the camera sensor with very little processing. These files are quite large and must be converted to JPEG, TIFF, or another file format before they are ready to use since many types of software do not support RAW images. TIFF files have a lossless compression algorithm, so their files are much larger than JPEG, but they have undergone demosaicing.

2.2. Colour Filter Array

To create colour images in digital cameras, three primary colours must be detected separately. The primary additive colours are red, green, and blue, while the primary subtractive colours are cyan, magenta, and yellow. Additive colour is used when light needs to emit different shade of colour, while subtractive colour is used when white light reflects off a coloured surface. Additive colour is used for cameras, as well as television

and computer screens, while subtractive colour is used for things like printing images. Cameras use additive colour by having different filters that are each sensitive to red, green, and blue, this is called a "colour filter array".

2.2.1. Bayer Pattern

In most cameras, including Canon, the colour filter array used is called a "Bayer filter" or "Bayer Pattern", named after Bryce E. Bayer [19]. The pattern is a repeating 2-by-2 grid consisting of two green cells, one red cell, and one blue cell, shown in Figure 2.4. Notice that there will be twice as many cells detecting green as there are detecting either red or blue. The reason for this is that the human visual system detects differences in luminance from the green portion of the spectrum, while colour perception is associated with the red and blue portions of the spectrum, meaning the human eye is more sensitive to green light [2].
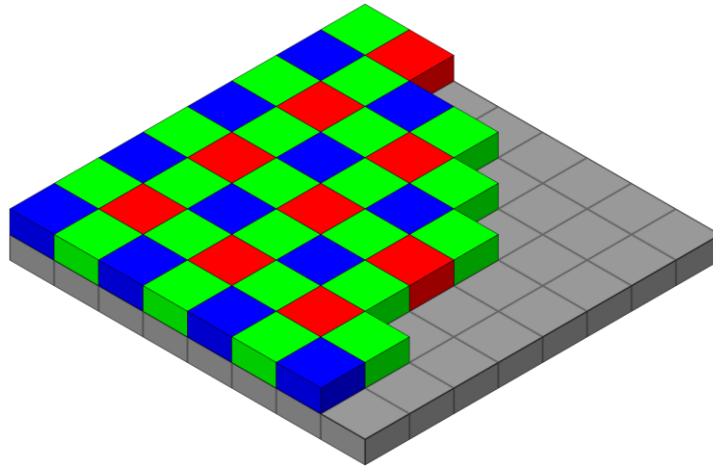
Figure 2.4: Bayer Filter Example. Taken from [20]

To reconstruct the image an interpolation algorithm called demosaicing is used. The exact algorithm can vary, however common methods include nearest-neighbour interpolation, bilinear interpolation, bicubic interpolation, and spline interpolation. The simplest of these is nearest neighbour interpolation, where the value for a certain pixel is simply taken from an adjacent pixel. Bilinear interpolation is the next simplest, where a

pixel value is calculated from the average of the adjacent pixels. When choosing which interpolation algorithm to use, there is a trade-off between quality and simplicity. The simplest algorithms will be quick to perform but will result in a lower quality image, perhaps with artifacts (distortion) introduced. Additionally, these algorithms do not account for defects from the sensor, such as SEUs, meaning the algorithm will cause the defects to spread to a larger area and become more noticeable in the final JPEG image. When the Bayer filter is used to record images, the colour of any SEUs that are displayed does not imply that the SEU was in fact that colour. The colour will simply result from which colour cell the SEU occurred in since the camera will interpret this as light of that colour, when in reality it is a defect that randomly hit a cell of that colour.

2.3. Single Event Upsets in Digital Imagers

2.3.1. Detection of Single Event Upsets

Single event upsets in digital cameras manifest as a single bright pixel, or a collection of bright pixels that appear in a single image but are not in images taken immediately before and after. To detect SEUs a series of long exposure photos must be taken and then photos are analyzed to locate any pixels that "light up" in a single image. Using the example in Figure 2.5, the algorithm starts by looking for any pixels that appear significantly brighter in Image i + 1 than in Image i, next it would check if those pixels appeared dark again in Image i + 2. If the pixel exhibits the behaviour shown in Figure 2.5, it would be classified as an SEU. Note that the SEU can also manifest as a cluster or streak of bright pixels, such as in Figure 1.5, not just a single pixel. The SEU detection algorithm will be discussed more in Chapter 3.

Image i   Image i + 1   Image i + 2
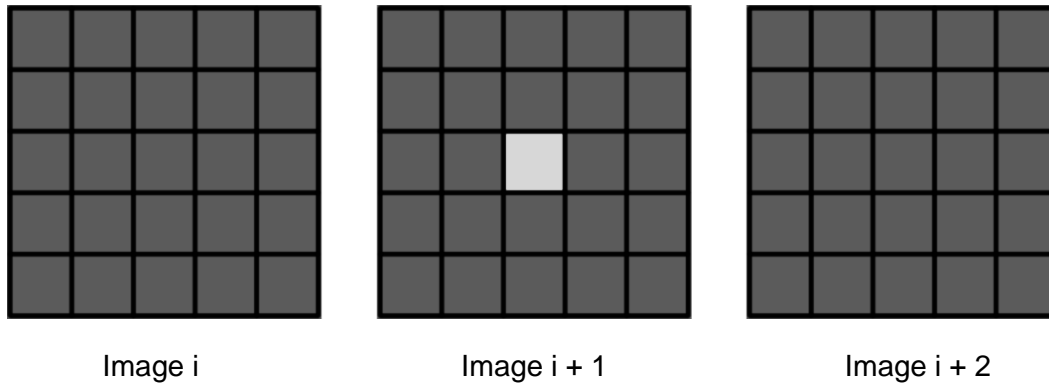
Figure 2.5: Example of an SEU in a Series of Images

2.3.2. Detection of SEUs at Varying Elevations with DSLR Cameras

The following chapters will discuss the relationship between elevation and SEU rates in greater detail. In previous research [13], [21] SEU detection methods in digital cameras were refined using MATLAB, and some preliminary experiments were conducted to document the relationship between elevation and rate of SEUs in digital imagers, however that research was more limited in the range of elevations and number of cameras used. This thesis will elaborate on that research by gaining more insight into how elevation affects SEU rates.

2.4. Summary

This chapter details the important settings on a DSLR camera, such as ISO, exposure time, and aperture, and how they can be manipulated. Colour filter arrays and the Bayer pattern were also introduced, explaining how they work for the camera to form an image. Additionally, background knowledge on single event upsets and the previous research on them was detailed.

Chapter 3.

Method

3.1. Overview

In this chapter the method to collect data and the algorithm to analyze it for SEUs will be discussed. First the process of using an intervalometer, essentially a program which takes a series of photos, will be described. Three cameras were used in this thesis, a Canon T2i, a Canon 5D Mark II, and a Canon 5DSR, all with similar but slightly different specifications.

3.2. Procedure to Capture Images

To collect data on SEUs in digital cameras, a series of photographs are taken with DSLRs and then analyzed in MATLAB. The type of images used are called "dark frames" meaning the camera sensor receives no illumination. This is done by adding a body cap to the camera body and containing it in a dark box. A body cap is essentially the same as a lens cap, however it is used when you remove the lens from a DSLR camera. After you remove the lens, the body cap attaches to the camera where the lens would normally go and blocks most light from hitting the sensor. Keeping the camera in a dark box also prevents any light from entering the camera through the eyepiece, which can illuminate the sensor slightly. Often, in photography dark frame subtraction is a technique used to remove noise from images. The photographer will take a dark frame image (or a series of dark frame images and average them) to get a baseline for the amount of noise in photos from that specific camera. This dark frame picture will display the thermal noise and hot pixels in the camera (technically it will also show any SEUs but since these are transient photographers cannot remove them with this technique) and can then be subtracted from any light frame photos taken with the camera to remove noise [22]. For the purposes of this thesis, the dark frame images taken should display only the SEUs, as well as any hot pixels or thermal noise present.

3.2.1. Overview of Procedure and Camera Background

In total, three cameras will be used to capture images, all with similar procedures. For one batch, 1000 photos are taken, each with an exposure time of 30 seconds, and with a pause of 60 seconds in between each photo. Since thermal noise increases with temperature [23], the 60 second pause between shots allows time for the camera sensor to cool down sufficiently. Another possible solution proposed to combat thermal noise is keeping the camera inside a temperature-controlled chamber [23], such as a refrigerator. However, this was not feasible since most of the time the camera is connected to a computer while shooting. Additionally, while shooting at high altitudes, there was no refrigerator available.

The three cameras used to record images are: a Canon 5DSR, a Canon 5D Mark II, and a Canon T2i. Basic specifications for these cameras are listed in Table 3.1 below.

Table 3.1: Image Sensor Size and Effective Pixels for Cameras [24]–[26]

Camera	Image Sensor Size	Effective Pixels	Pixel Size
Canon 5DSR	36.0 mm × 24.0 mm	50.60 megapixels	4.14 µm
Canon 5D Mark II	36.0 mm × 24.0 mm	21.10 megapixels	6.41 µm
Canon T2i	22.3 mm × 14.9 mm	18.00 megapixels	4.30 µm

All three cameras are DSLRs with removable lenses, meaning the cameras can be separated into two pieces: the camera body, and the camera lens. When recording the images, the lens is removed from the camera and a body cap is attached to cover the sensor. This blocks a significant amount of illumination from reaching the sensor. To block out even more illumination, the camera is stored inside either a camera bag or a box with a lid. If conditions permit, the camera inside the bag or box is ideally placed in a cool, dark location while a computer controls the camera. These steps are taken to minimize the illumination of the sensor and to minimize thermal noise.

Adjustable settings on the DSLR cameras include ISO and exposure time. For capturing photos for SEU detection, a long exposure time of 30 seconds is used. A variety of ISOs are used, starting at ISO 1600, and increasing up to ISO 12800, or the highest ISO the camera allows.

3.2.2. Intervalometer Software

To record the images an intervalometer is used, which triggers the camera to take a series of photos, setting the number of photos, photo parameters, and pause between the pictures. Four different intervalometer programs are used: Astro Photography Tool, Canon EOS Utility, Magic Lantern, and the built-in intervalometer on the Canon 5DSR.

Astro Photography Tool (APT) is a computer program designed specifically for astrophotography [27], but it works seamlessly to record images for SEU detection. It includes an intervalometer that allows the user to program a "plan" to take a series of photos and set different parameters. For the plan, the user can set what ISO and exposure time to use, how many photos to take, and the delay time between photos. The plan can also include changes in parameters, for example, it can take 1000 photos at ISO 1600 and then switch to ISO 3200 and take another 1000 photos. Any of the parameters can automatically be changed at any point during the plan, however, for the purpose of detecting SEUs, ISO is the only parameter within the camera that changes during the duration of the plan.

Canon EOS Utility is another computer application which includes an intervalometer, however, unlike APT, you cannot program it to change parameters automatically. When using either APT or EOS Utility, the camera must be connected to a computer, and the photos can be stored to either the computer or to external storage, such as an SD card or external hard drive. Generally, when using APT and EOS Utility the photos were saved directly to a hard drive to because of the large volume of files generated.

Next, Magic Lantern is a firmware add-on made for Canon DSLRs and can be run through the SD card in the camera [28]. It includes many features that are not already available on the camera, such as an intervalometer. This add-on was only used for the Canon T2i since it wasn't needed for the other cameras. The program must be loaded onto an SD or CF card, then the card must be inserted into the camera and a firmware update must be performed to install the program. Once installed, the intervalometer allows you to simply take a specified number of photos at a single ISO.

For the Canon 5DSR, the built-in intervalometer was also used, since the 5DSR was the only camera with a built-in intervalometer. For this the user chooses their settings,

such as ISO, exposure time, and the pause between photos. Then the intervalometer runs until the user disables it or the battery dies. The user can also select the number of photos taken, but the maximum option is 99 frames and for this thesis 1000 frames were generally taken, so this setting was not used.

3.2.3. Combinations of ISOs and Elevations Studied

Since a different combination of ISOs and software was available for each camera, Table 3.2 below lists which ISOs were used for each camera, and what software was used to capture the images. For the Canon T2i, the ISOs do not include ISO 12800 since this camera only goes up to ISO 6400.

Table 3.2: List of Cameras with ISOs Used for Capturing Photos and Intervalometer Software Used

Camera	ISOs Used	Intervalometer Software Used
Canon 5DSR	1600, 3200, 6400, 12800	APT, Built-In Intervalometer
Canon 5D Mark II	1600, 3200, 6400, 12800	APT, EOS Utility
Canon T2i	1600, 3200, 6400	APT, EOS Utility, Magic Lantern

Taking 1000 photos with an exposure time of 30 seconds and a pause between photos of 60 seconds takes a total of 1500 minutes, or 25 hours. A regular camera battery would only last for a few hours, so instead a DC coupler replaces the battery pack and provides uninterrupted power to the camera while the DC coupler is plugged into an outlet.

To collect images at different elevations, a variety of locations near Vancouver, BC where there is a large range of elevations within a moderate radius were used. Since many locations were used, with the two farthest being approximately 200 kilometres from each other, there is a possibility that the number of SEUs was affected by location, however my thesis will focus on differences seen at different altitudes. Not all cameras were used at each location due to time and software constraints, Table 3.3 below lists what cameras were used at each elevation, and the location.

Table 3.3: List of Cameras and Locations for Elevation Analysis

Elevation	Cameras Used	Location	Latitude and Longitude
5 m	Canon 5DSR, Canon 5D Mark II, Canon T2i	Port Coquitlam, BC	49°15'42.202" N, 122°45'9.167" W
77 m	Canon 5D Mark II	Burnaby, BC	49°17'1.239" N, 123°0'27.307" W
117 m	Canon 5DSR, Canon 5D Mark II, Canon T2i	Burnaby, BC	49°17'7.348" N 122°58'35.729" W
238 m	Canon 5DSR, Canon 5D Mark II, Canon T2i	North Vancouver, BC	49°21'4.875" N 123°1'37.127" W
366 m	Canon 5DSR, Canon 5D Mark II, Canon T2i	Burnaby, BC	49°16'37.687" N 122°54'48.918" W
719 m	Canon 5DSR, Canon 5D Mark II, Canon T2i	Sunshine Valley, BC	49°16'23.529" N 121°14'18.876" W
921 m	Canon 5DSR	West Vancouver, BC	49°23'46.968" N 123°12'17.317" W
1194 m	Canon 5DSR, Canon 5D Mark II, Canon T2i	Manning Park, BC	49°3'49.986" N 120°47'12.737" W

Since latitude also affects the occurrence rate of cosmic rays [10], Table 3.3 lists the coordinates of the locations used. You can see that all locations for the camera were at approximately 49° N. There is a range of only about 20 arcminutes, which is approximately a 30-kilometre difference in altitude, calculations for this, as well as a more detailed description of what arcminutes are, is shown in Appendix A.

3.3. SEU Detection Algorithm

The algorithm to detect SEUs in the raw images begins by calculating the average intensity and standard deviation of the intensity at each pixel address for the 1000 images. To calculate these values over the 1000 images, the values from each image must be summed one image at a time since MATLAB cannot handle storing 1000 images at once. In general, if there are m images, to find the mean the pixel intensity at each pixel address (x,y) is summed until all pixels for all m images have been added together, then the final sum is divided by the total number of images. The following formula shows how the mean of the pixel at coordinates (x,y) is calculated for m images.

$$Mean\ of\ Pixel\ (x,y) = \ \mu(x,y) = \frac{\sum_{n=1}^{m} Image\ n(x,y)}{m} \qquad (3.1)$$

To calculate the standard deviation of the pixel at (x,y), the following equation is used. Since the mean at (x,y) appears in the equation, the final mean from m images must first be found before any of the standard deviations can be found. For pixel (x,y), the intensity of that pixel minus the mean value of pixel (x,y) from m images is squared. This value is then added to a running sum. Once this value from all m images has been summed, the final sum is divided by m to give the variance. To get the standard deviation, the square root of the variance is taken.

$$Standard\ Deviation\ of\ Pixel\ (x,y) = \sigma(x,y) = \sqrt{\frac{\sum_{n=1}^{m}(Image\ n(x,y) - \mu(x,y))^2}{m}} \qquad (3.2)$$

These average and standard deviation values will be used later to get a baseline for the noise at each pixel location. Since the values have been found for a dataset of 1000 images, any defects will have a very slight effect on the mean at each pixel, therefore the mean and standard deviations give a very good idea of what levels of noise are expected for each pixel in the imager.

Previous SEU detection algorithms did not calculate the mean and standard deviation for every pixel in the imager, rather they relied on a threshold for the noise of the

entire image. This major issue with that algorithm is that noise drastically differs in different areas of the imager. Figure 3.1 below shows an example of a noise map, specifically for the Canon 5D Mark II at ISO 12800 with an exposure time of thirty seconds. The noise at each individual pixel is not shown, but rather boxes that show the average intensity of the noise in different sections of the photograph. The noise map will differ significantly from camera to camera and will change slightly as ISO or exposure time is adjusted. For the same camera, if the ISO and/or exposure time is changed the general pattern of the noise map will hold, but the intensity values for the noise will increase accordingly.
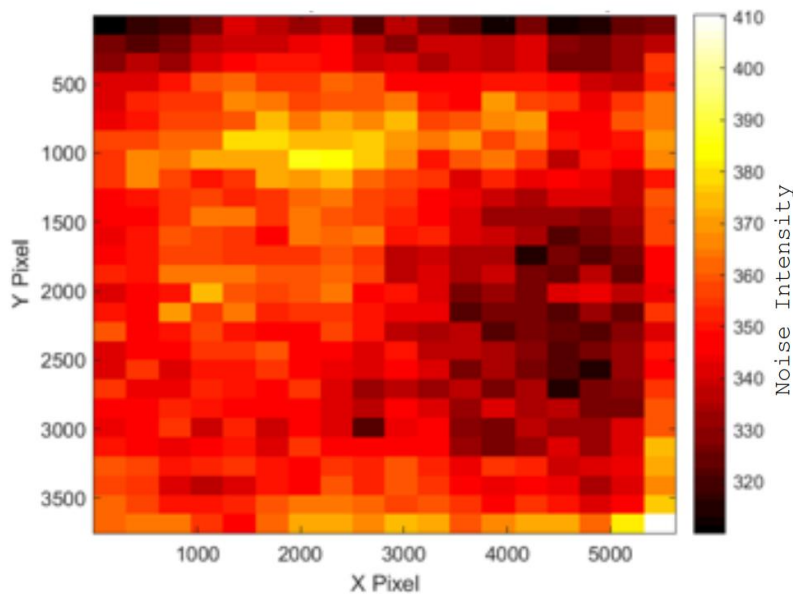
Figure 3.1: Noise Map from Canon 5D Mark II (ISO 6400). Taken from [13]

Using the method of finding the noise at each pixel address allows for weak SEUs to be detected and prevents noise from being falsely detected as SEUs. The main drawback to this method is the computation time, as the computation time directly correlates to the number of SEUs in the image, it can take anywhere from one to five hours to run the MATLAB code for 1000 images. Since at higher ISOs more SEUs are detected (because much weaker SEUs can be seen), higher ISOs also correspond to higher computation times.

Beginning with the second image in the batch, the algorithm compares each image to the previous and next images. First the difference between the intensity at each pixel in the current image and the previous image is found, as in the equation (3.3) below where i denotes the current image, i-1 is the previous image and (x,y) are the coordinates of the pixel in question.

$$Difference_i(x,y) = Image_i(x,y) - Image_{i-1}(x,y)$$ (3.3)

Any pixel addresses which fit equation (3.4) are flagged. This step checks that a given pixel in a single image is illuminated more than expected. This could potentially be an SEU, however it could also be noise or a hot pixel at this point.

$$Difference_i(x,y) > Threshold \quad and \quad Image_i(x,y) > \mu(x,y) + 5\sigma(x,y)$$ (3.4)

The value of mean plus four standard deviations is used since statistically, this will give a 1 in 3,488,556 chance [29] of being randomly occurring data, and not caused by an SEU. In previous detection algorithms, only the threshold portion of equation (3.4) was used, which caused many noisy pixels in low noise areas of the sensor to be falsely detected as SEUs. By calculating the noise at each pixel, this algorithm is able to detect weak SEUs in low noise areas and strong SEUs in any high noise areas.

Next, the intensity of the same pixel in the previous and following images is compared to equation (3.5).

$$Image_{i-1}(x,y) < \mu(x,y) + 4\sigma(x,y) \quad and \quad Image_{i+1}(x,y) < \mu(x,y) + 4\sigma(x,y)$$ (3.5)

Now, instead of four standard deviations, five is used, which instead gives a 1 in 31,574 chance [29] chance of the intensity value being random data that does not fit equation (3.5). This determines if the same pixel in the previous and following images appears relatively unilluminated. If it is in fact dark the pixel continues to be flagged as a potential SEU, otherwise, if it is illuminated, it is likely a hot pixel or simply noise and can be ignored. Now all SEUs have been flagged and recorded.

Next, to locate any SEU clusters or streaks, the algorithm looks for any SEUs previously found that are within a distance of 6 pixels of each other, in both the horizontal and vertical direction. If there are any, they will be classified as "clusters". This algorithm does not differentiate between streaks and clusters, and simply combines the two into the category "clusters".

3.4. Summary

In this chapter, the procedure for accumulating datasets of images was discussed in detail, followed by the algorithm used to locate SEUs in the images. Intervalometer software for the three cameras used was explained along with brief specifications for the cameras as well as the various altitudes studied. The algorithm for locating SEUs is discussed, explaining how a baseline for the noise levels in a set of photos is found and then how that baseline is used to more accurately determine which pixels contain SEUs. The following chapter will discuss the results of these experiments and the relationship between occurrence rates of SEUs and elevation.

Chapter 4.

Results and Analysis

4.1. Overview

Previous chapters described the history behind SEUs, as well as the experimental methods for collecting data and the algorithm to detect SEUs in dark frame images. This chapter will examine the results of how SEUs behave at different elevations. The number of SEU occurrences in datasets of 1000 images will be given for each elevation, ISO, and camera, and compared to neutron flux theory. Then the SEU occurrence rates, given as how many SEUs occur for a given amount of time, compared to the area of the camera sensor, will be calculated. Next, histograms of the SEU charge distribution for the various cameras will be presented. Finally, some interesting deviances from expected results will be discussed and the cause of these will be hypothesized.

4.2. Findings from Previous Research

In determining the basis for this research, prior research [13] was looked at as a foundation for conducting experiments. Previously, the change in occurrence rates of SEUs with respect to elevation was only briefly covered. Only two cameras, the Canon 5D Mark II and the Canon T2i, were used at only four elevations, with the highest being 366 metres above sea level. Further research [12] added a fifth elevation of 1088 metres, however this was only done with the Canon 5D Mark II. In this thesis, a third camera was added to the experiments, as well as adding several higher elevations with a maximum of 1194 metres above sea level, which gives more data points at a wider range of elevations. The new tests were performed at a total of eight different elevations, with each camera having data from at least six of those eight elevations. The only drawback here is that with the additional elevations added, a wider variety of locations were used, meaning changes in latitude could possibly affect the results more than they had in previous research. Previously, the latitudes only had a range of approximately 8 arcminutes, whereas now there is a range of 20 arcminutes. However, section 3.2.3 covers how the changes in

latitude between locations are relatively small, and therefore unlikely to influence the results significantly, since even 20 arcminutes is equivalent to only 30 kilometres.

4.3. Experimental Results

Using the procedure and analysis method described in sections 3.2 and 3.3 datasets of photographs were collected and analyzed to detect SEUs. For each of the three cameras, the Canon T2i, Canon 5D Mark II, and the Canon 5DSR, experiments were conducted at ISOs ranging from 1600 to 12800, or in the case of the Canon T2i, to ISO 6400, the highest available ISO for that camera, and up to eight different elevations per camera. In some cases, fewer than 1000 photos were taken, mainly due to time constraints caused by higher elevations being difficult to access. When determining SEU occurrence rates, the error of the rates will decrease proportional $1/\sqrt{n}$, where n is the number of pictures taken, so the error does not increase drastically when the number of photographs is decreased to 600, or even to 350. Table 4.1 below lists how many photographs were taken at each elevation for each camera. Note that approximate numbers are listed for elevations about 366 metres, since the exact number varied slightly across each ISO.

Table 4.1: Summary of Image Datasets Collected

Elevation	Canon T2i	Canon 5D Mark II	Canon 5DSR
5 m	1000	1000	1000
77 m		1000	
117 m	1000	1000	1000
238 m	1000	1000	1000
366 m	1000	1000	1000
719 m	600	350	350
921 m			600
1194 m	350	170	170

Note that some of the cells show that zero photographs were taken, the photographs taken at 77 metres were taken by another student, prior to my thesis and data from only one camera was available. At 921 metres, there was no access to a computer, so only the Canon 5DSR was able to be used since it has a built-in intervalometer. The Canon T2i was not used here because this was prior to when we began using Magic Lantern with the Canon T2i and therefore could not operate the intervalometer without a computer. Next, the following sections will describe the results of how SEUs behave at varying altitudes.

4.4. Number of SEU Occurrences in 1000 Images

First, the number of SEUs per centimetre squared in 1000 images will be plotted in relation to the elevation, for each combination of ISO and camera. Here the size or strength of the SEU is not a factor, only the total number of SEUs is displayed. Later, in section 4.6, the strength of SEUs will be discussed.

Figure 4.1 through Figure 4.11 display the SEU count per centimetre squared in 1000 images versus the elevation in metres. To find the SEU count per centimetre squared, the total number of defects in 1000 images was divided by the sensor area, which is 2.23 cm by 1.49 cm for the Canon T2i, and 3.6 cm by 2.4 cm for the Canon 5D Mark II and 5DSR. Note that for any elevations where 1000 images were not taken, the values displayed were scaled to give the SEU count per 1000 images. For example, if only 200 images were taken at a given elevation and ISO, then the number of events was multiplied by five to get the events per 1000 images. For clarity, the number of SEUs per 1000 images is displayed above each data point, as well as the equation of the linear regression line, which is displayed on the right side.

Figure 4.1: SEU Count vs. Elevation for Canon T2i (ISO 1600, T = 30s, Pixel Size = 4.30 µm, Effective Pixels = 18.00 megapixels, Sensor Size = 2.23 cm by 1.49 cm)
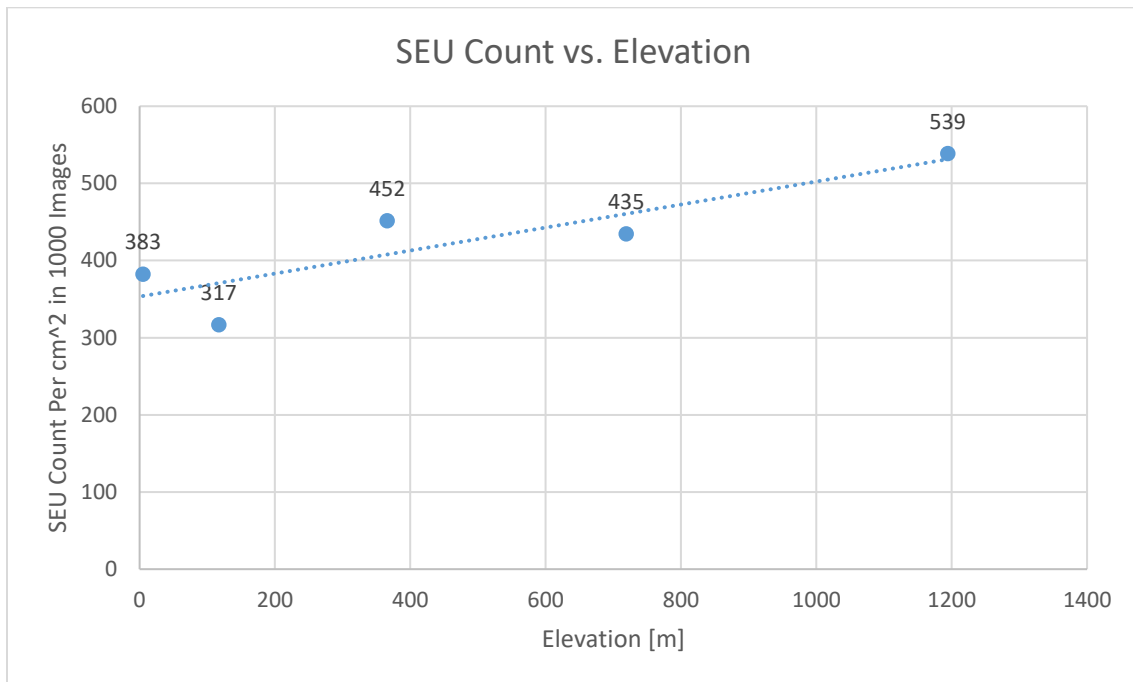
Figure 4.2: SEU Count vs. Elevation for Canon T2i (ISO 3200, T = 30s, Pixel Size = 4.30 µm, Effective Pixels = 18.00 megapixels, Sensor Size = 2.23 cm by 1.49 cm)
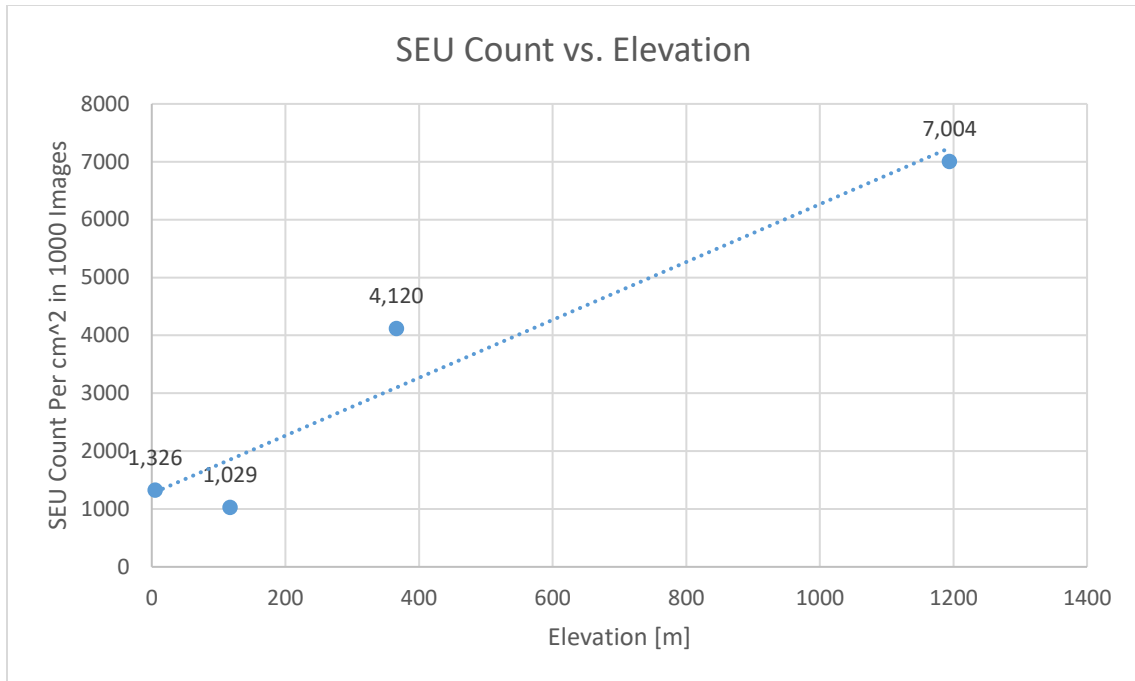
Figure 4.3: SEU Count vs. Elevation for Canon T2i (ISO 6400, T = 30s, Pixel Size = 4.30 μm, Effective Pixels = 18.00 megapixels, Sensor Size = 2.23 cm by 1.49 cm)
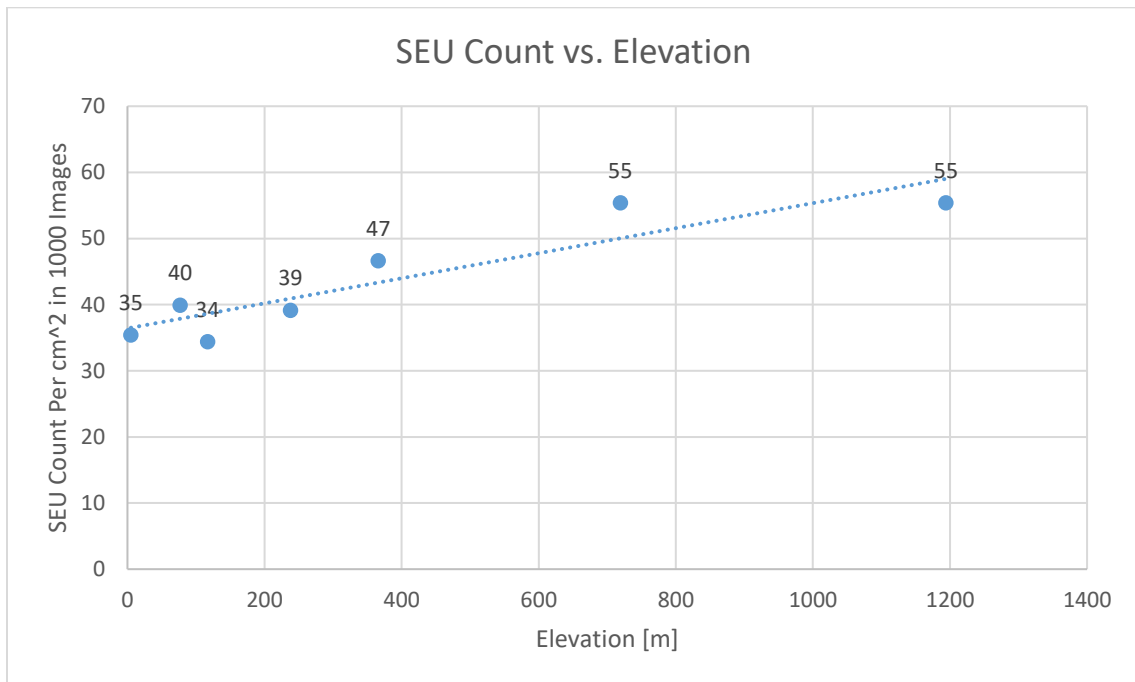
Figure 4.4: SEU Count vs. Elevation for Canon 5D Mark II (ISO 1600, T = 30s, Pixel Size = 6.41 μm, Effective Pixels = 21.10 megapixels, Sensor Size = 3.6 cm by 2.4 cm)

31
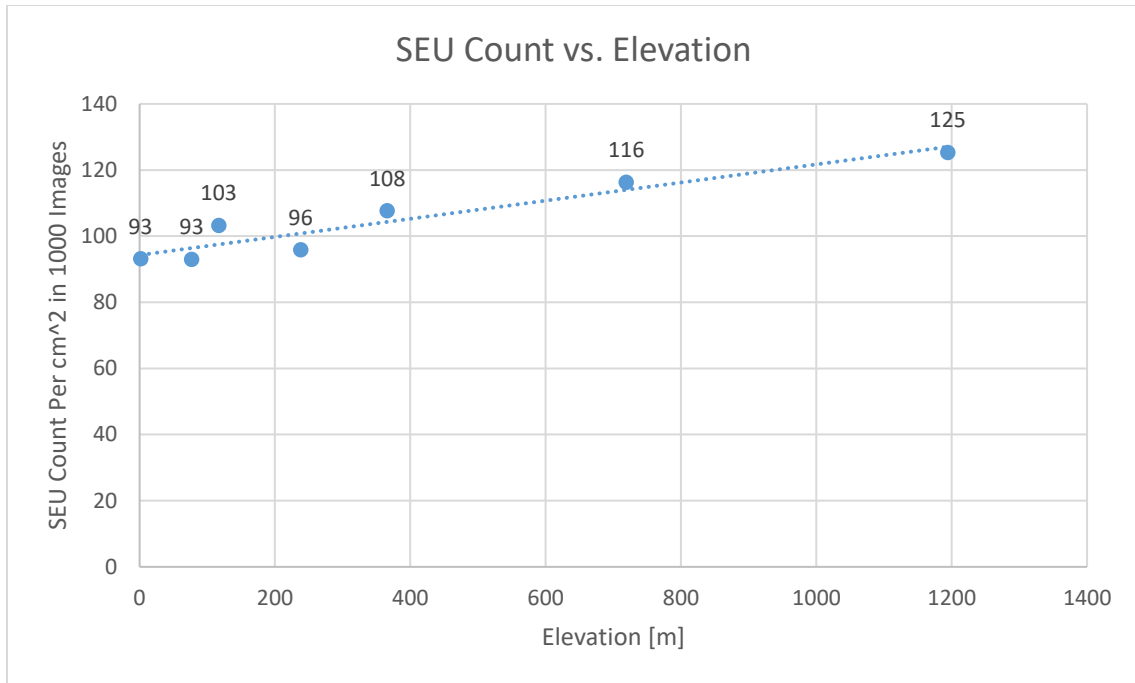
Figure 4.5: SEU Count vs. Elevation for Canon 5D Mark II (ISO 3200, T = 30s, Pixel Size = 6.41 µm, Effective Pixels = 21.10 megapixels, Sensor Size = 3.6 cm by 2.4 cm)
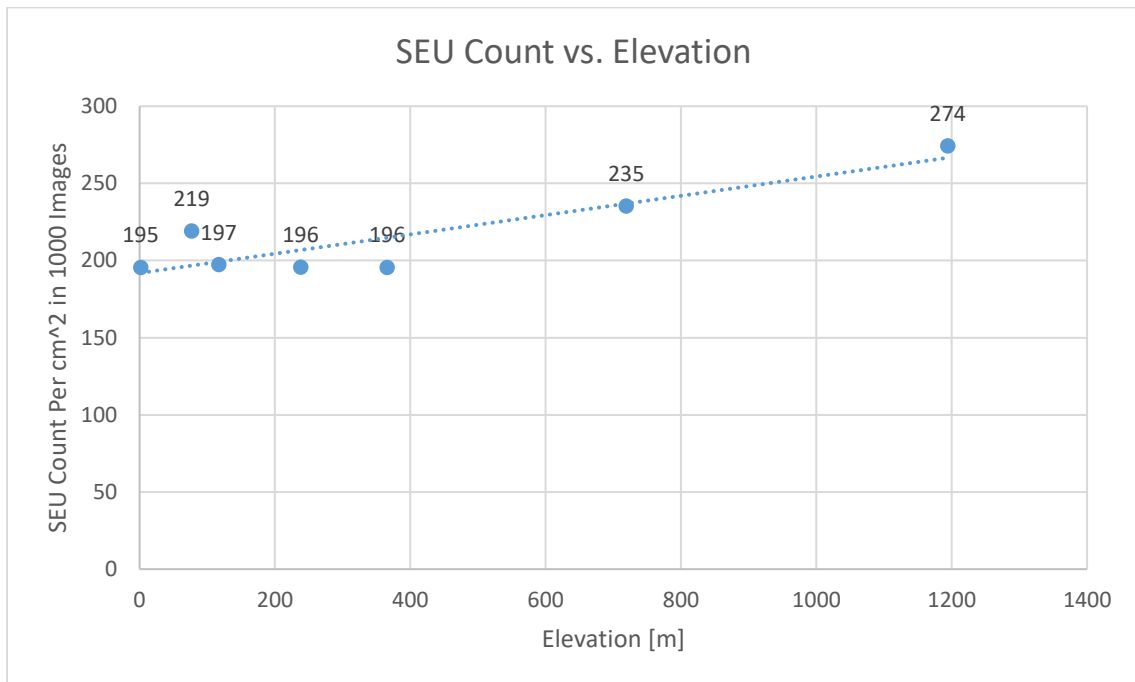
Figure 4.6: SEU Count vs. Elevation for Canon 5D Mark II (ISO 6400, T = 30s, Pixel Size = 6.41 µm, Effective Pixels = 21.10 megapixels, Sensor Size = 3.6 cm by 2.4 cm)
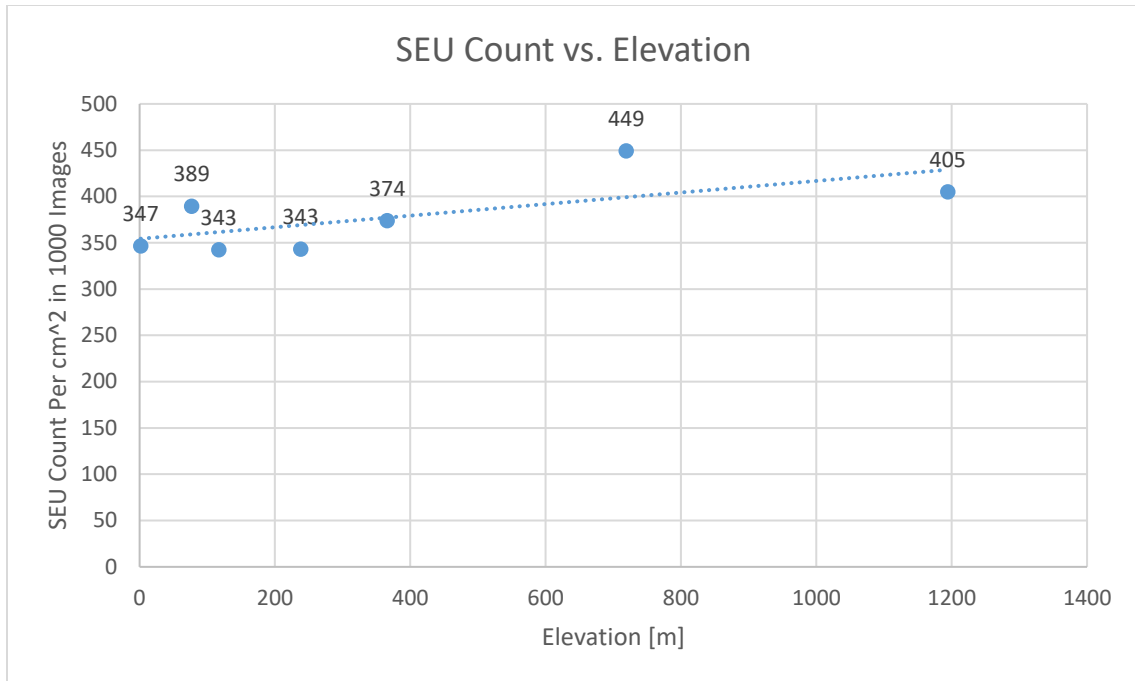
Figure 4.7: SEU Count vs. Elevation for Canon 5D Mark II (ISO 12800, T = 30s, Pixel Size = 6.41 µm, Effective Pixels = 21.10 megapixels, Sensor Size = 3.6 cm by 2.4 cm)
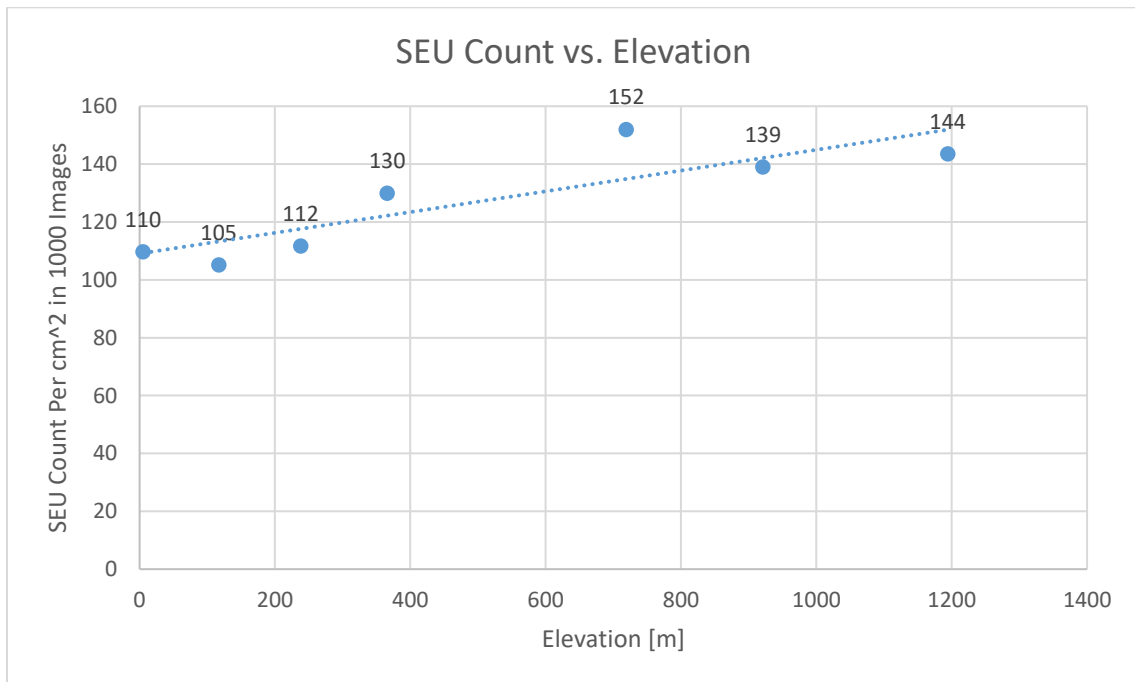
Figure 4.8: SEU Count vs. Elevation for Canon 5DSR (ISO 1600, T = 30s, Pixel Size = 4.14 µm, Effective Pixels = 50.60 megapixels, Sensor Size = 3.6 cm by 2.4 cm)
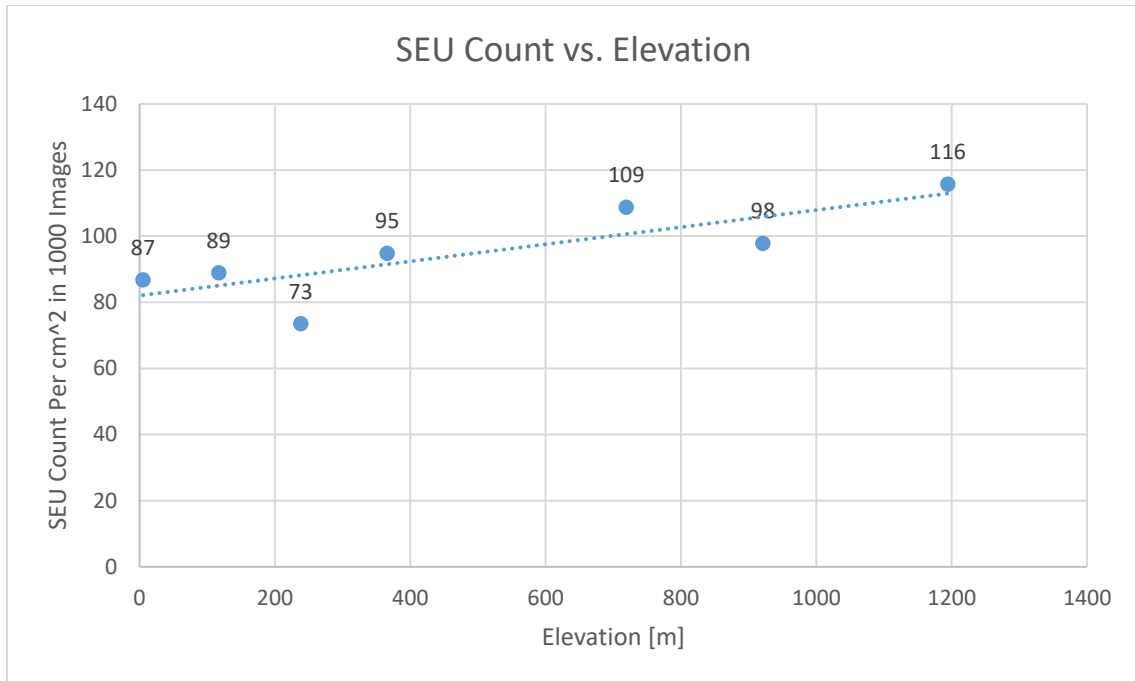
Figure 4.9: SEU Count vs. Elevation for Canon 5DSR (ISO 3200, T = 30s, Pixel Size = 4.14 μm, Effective Pixels = 50.60 megapixels, Sensor Size = 3.6 cm by 2.4 cm)
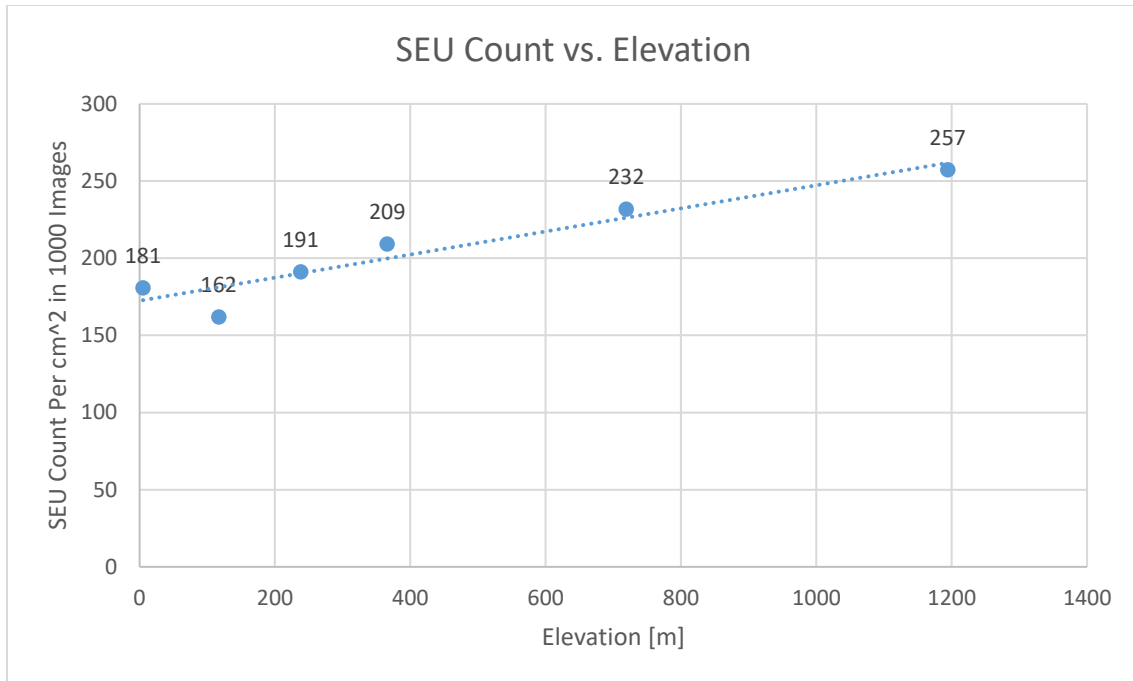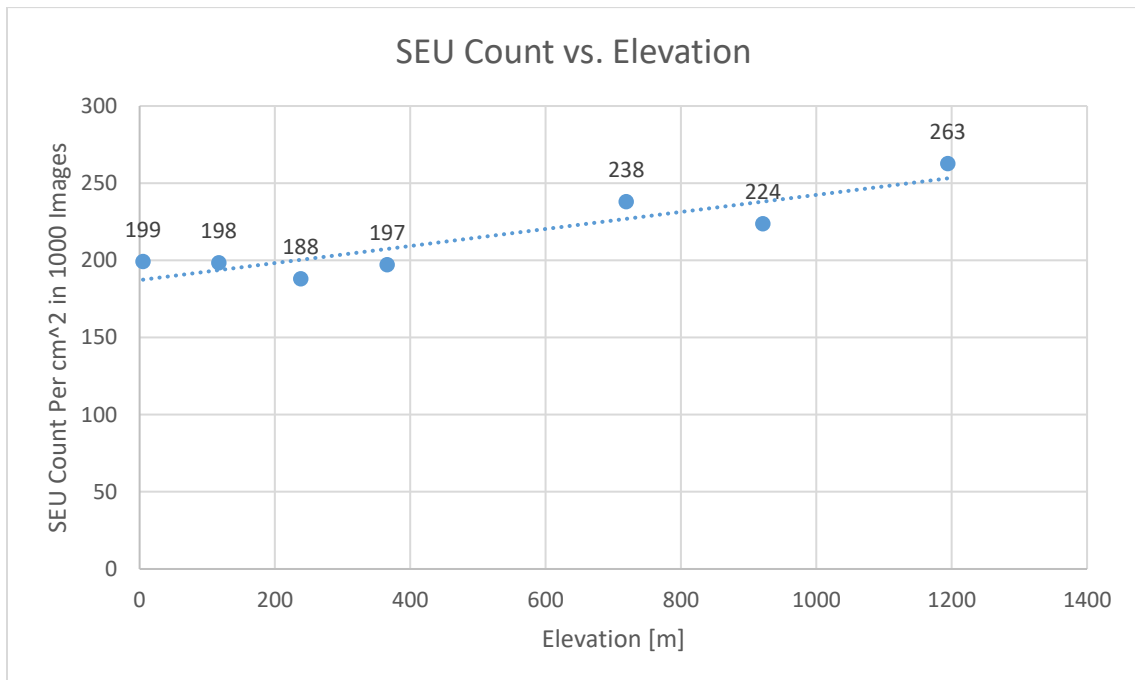

Figure 4.10: SEU Count vs. Elevation for Canon 5DSR (ISO 6400, T = 30s, Pixel Size = 4.14 μm, Effective Pixels = 50.60 megapixels, Sensor Size = 3.6 cm by 2.4 cm)
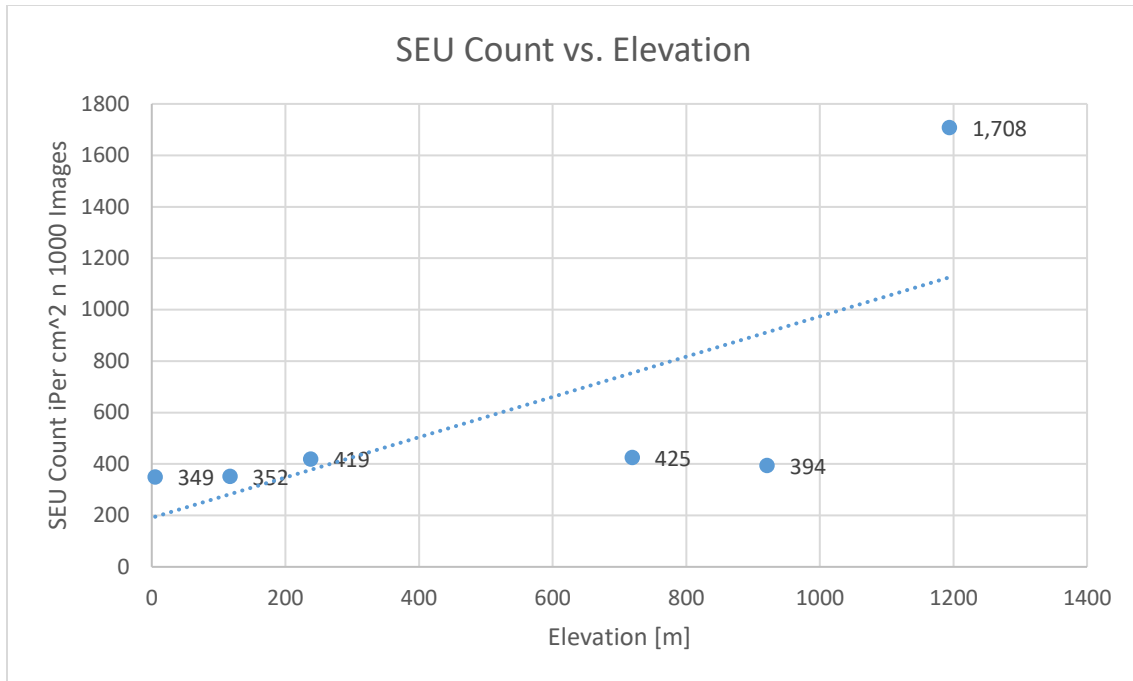
Figure 4.11: SEU Count vs. Elevation for Canon 5DSR (ISO 12800, T = 30s, Pixel Size = 4.14 μm, Effective Pixels = 50.60 megapixels, Sensor Size = 3.6 cm by 2.4 cm)

From the results of how SEU rates change when altitude increases, we can see that overall, SEU rates tend to increase with altitude, as expected. However, there were some individual points where the SEU occurrence rate was lower for higher altitudes. Looking at the second and third points on the graph in Figure 4.10, it is apparent that there was a 5.5% decrease in the total number of SEUs even though there was a 121-metre increase in elevation. Possible explanations for these deviances could be changes in latitude between where the experiments were performed, or more likely variations in solar weather from one day to another, or throughout the day.

The general relationship shown as ISO doubles is most SEU rates increase by a factor of between 1.7 to 2.6 times, for a given elevation. Similarly, the y-intercept approximately doubles when ISO is doubled, although the change in y-intercept for different ISOs varies more than the slope does. However, there are cases that deviate from this, specifically at high ISOs and high elevations. For example, in Figure 4.6 the data at ISO 6400 has a much greater slope than at ISO 1600 or 3200 in Figure 4.4 and Figure 4.5. This is also apparent in Figure 4.11 where there is approximately a 500% increase in

SEU rates between sea level and 1194 metres. Comparing this to data from the same cameras at lower ISOs, there is only around a 30-40% increase in SEU rates between sea level and 1194 metres. This is likely due to the increased noise at high ISOs since it occurs at the maximum ISO for the Canon T2i and 5DSR. To determine if it is in fact noise that is being falsely detected as SEUs, the charge distribution of the detected SEUs can be plotted and will be discussed later, in section 4.6.

Similarly, in Figure 4.11 the data at ISO 12800 has a much higher slope than the other ISOs. Here, the data point at 1194 metres is much higher than expected and has a huge influence on the linear regression line. Ideally the test at this elevation and ISO should be redone, but since it is hard to access that elevation, it was not.

Another unexpected result is if you look at Figure 4.8 and Figure 4.9, you will notice that the data for ISO 1600 in fact has more SEUs than the data for ISO 3200, and this pattern holds for all seven elevations. Initially, this seemed like a mistake, however after double checking all the data was correct, the Canon 5DSR did in fact detect more SEUs with ISO 3200 than ISO 1600. The reason for this is unknown, however one possibility could be any built-in noise suppression algorithms in the camera. It is also interesting that this behaviour was not recorded for any other ISOs or other cameras.

To determine how reliable the linear regression lines form the data are, the slopes and y-intercepts as well as their respective standard errors are listed below in Table 4.2 through Table 4.4.

Table 4.2: Slope and Y-Intercept Values for Canon T2i (T = 30s, Pixel Size = 4.30 µm, Effective Pixels = 18.00 megapixels, Sensor Size = 2.23 cm by 1.49 cm)

ISO	Slope	Slope Error	Y-Intercept	Y-Intercept Error
1600	0.07	±0.01 (±20%)	172	±7 (±4%)
3200	0.15	±0.05 (±30%)	350	±30 (±9%)
6400	5	±1 (±20%)	1300	±600 (±50%)

Table 4.3: Slope and Y-Intercept Values for Canon 5D Mark II (T = 30s, Pixel Size = 6.41 µm, Effective Pixels = 21.10 megapixels, Sensor Size = 3.6 cm by 2.4 cm)

ISO	Slope	Slope Error	Y-Intercept	Y-Intercept Error
1600	0.019	±0.004 (±20%)	36	±2 (±6%)
3200	0.027	±0.004 (±10%)	94	±2 (±2%)
6400	0.06	±0.01 (±20%)	192	±8 (±4%)
12800	0.06	±0.03 (±50%)	350	±20 (±5%)

Table 4.4: Slope and Y-Intercept Values for Canon 5DSR (T = 30s, Pixel Size = 4.14 µm, Effective Pixels = 50.60 megapixels, Sensor Size = 3.6 cm by 2.4 cm)

ISO	Slope	Slope Error	Y-Intercept	Y-Intercept Error
1600	0.036	±0.009 (±30%)	109	±6 (±6%)
3200	0.026	±0.008 (±30%)	82	±5 (±7%)
6400	0.06	±0.01 (±20%)	187	±8 (±4%)
12800	0.8	±0.4 (±50%)	200	±300 (±200%)

If you focus specifically on the highest ISO for each camera, it is apparent that the error in both the slopes and y-intercepts are huge. When the percent error in the slope is 30% or less, this indicates a good fit, however as the percent error increases past 50%, it indicates a much poorer fit. This hints that the data at the highest ISOs is not statistically significant, so in the future it is probably unnecessary to record any photos at the highest ISO for a given camera, since there appears to be too much noise to extract any usable data.

Lastly, if the parameter of pixel size is considered, the Canon T2i and 5DSR have similar pixels sizes of 4.30 µm and 4.14 µm respectively, while the Canon 5D Mark II has a pixel size of 6.41 µm, so the 5D Mark II can be compared to the other two cameras. From the standard error values for slope and y-intercept, it is apparent that for the most part the ratio of standard error to the slope or y-intercept is smaller than for the Canon T2i and 5DSR. Essentially this means that for smaller pixel sizes, the data has slightly more variation, likely caused by an increase in noise for smaller pixels sizes.

4.4.1. Neutron Flux Theory

At high elevations, there is a decrease in air density, which allows for a rise in neutron flux, causing an increase in cosmic particles. This explains why SEU rates increase with elevation. A 1996 paper by J. F. Ziegler [5] detailed the behaviour of cosmic rays near Earth and gave a relationship for the rates of cosmic rays at different elevations. In a more recent and comprehensive paper from 2004 by M. S. Gordon et al. [30] research was done on neutron flux and the experiments resulted in the same relationship between elevation and rates of cosmic rays as the paper by Ziegler. The data on SEU rates at varying elevations can be compared to this model for how neutron flux depends on elevation. Equation (4.1) below expresses the ratios of neutron flux at two given altitudes [5], [30].

$$\frac{I_2}{I_1} = e^{\frac{A_1 - A_2}{L}} \tag{4.1}$$

Where I_2/I_1 is the ratio of the neutron flux at altitudes A_2 and A_1, and L is the absorption length, or attenuation factor, which is equal to $148 \; g/cm^2$ for neutrons. Here A is expressed in g/cm^2, which can be converted from metres using the following equation where H is the height in metres [5].

$$A = 1033 - 0.01112H + 3.96 * 10^{-8}H^2 \tag{4.2}$$

For elevations in the same range as those studied in this thesis, the ratio I_2/I_1 is plotted in Figure 4.12 below.
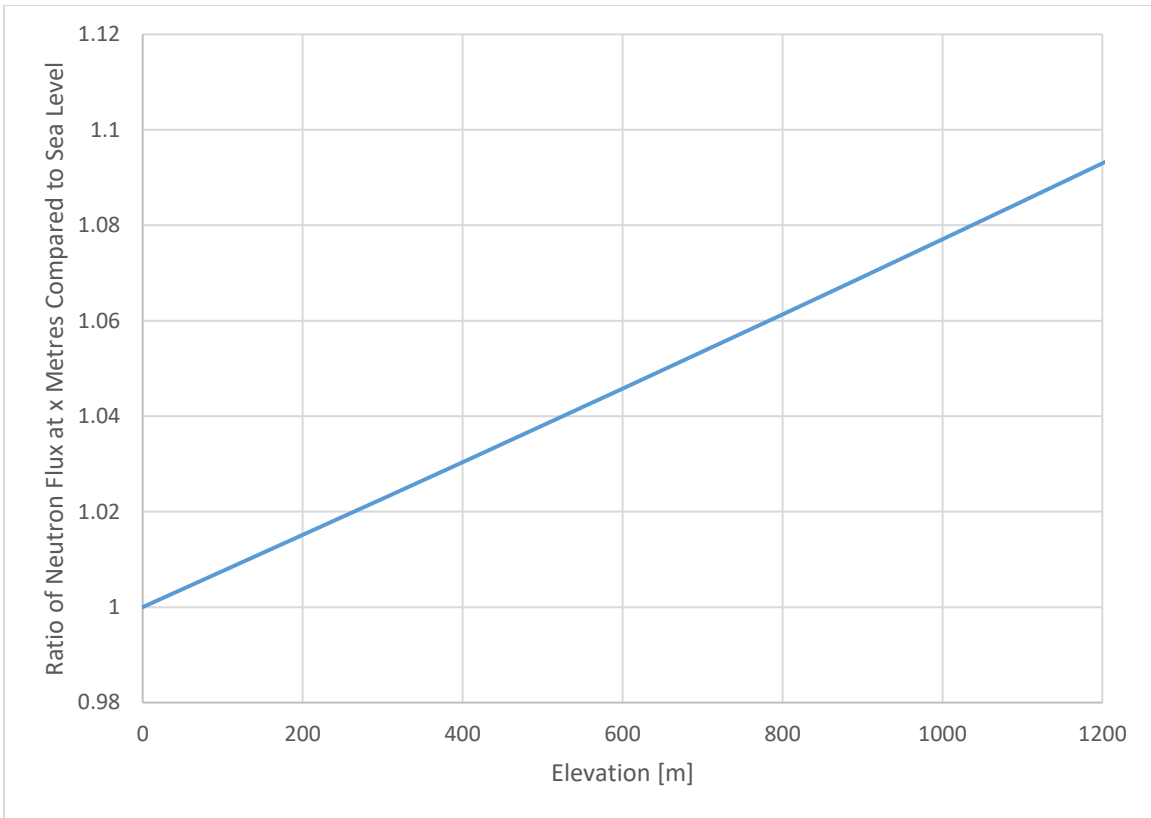
Figure 4.12: Neutron Flux Ratio Compared to Elevation

Notice that the plot appears perfectly linear, while equation (4.1) is not a linear equation. This is because the relationship only begins being non-linear at very high elevations, above around 20,000 metres. Therefore, the neutron flux theory helps to explain why the relationship between SEUs detected and elevation is linear, at least for modest elevations.

4.5. SEU Occurrences per Second

A more intuitive method of displaying the same data as above is to calculate the SEU occurrence rate per second per centimetre squared. To calculate this, the total number of SEUs in 1000 images must be divided by the time it takes to record 1000 images and then divided by the area of the sensor, in centimetres squared. As mentioned previously, it takes 25 hours to record 1000 images, however most of this time is attributed

to the pause between photographs, which must be ignored in the calculation. The time the camera is capturing images for, if 1000 exposures are taken at 30 seconds each will then be 30,000 seconds. As the sensor size varies between cameras it is listed in the second row of Table 4.5 to Table 4.8.

Table 4.5: SEU Rate Per Second Per Centimetre Squared at Different Elevations at ISO 1600

Camera	Canon T2i	Canon 5D Mark II	Canon 5DSR
Sensor Size [cm x cm]	2.23 x 1.49	3.6 x 2.4	3.6 x 2.4
Rate per Second at 5 m	0.0060	0.0012	0.0036
Rate per Second at 77 m		0.0014	
Rate per Second at 117 m	0.0054	0.0012	0.0035
Rate per Second at 238 m	0.0063	0.0013	0.0037
Rate per Second at 366 m	0.0069	0.0015	0.0043
Rate per Second at 719 m	0.0078	0.0019	0.0051
Rate per Second at 921 m			0.0046
Rate per Second at 1194 m	0.0084	0.0019	0.0047

Table 4.6: SEU Rate Per Second Per Centimetre Squared at Different Elevations at ISO 3200

Camera	Canon T2i	Canon 5D Mark II	Canon 5DSR
Sensor Size [cm x cm]	2.23 x 1.49	3.6 x 2.4	3.6 x 2.4
Rate per Second at 5 m	0.013	0.0031	0.0029
Rate per Second at 77 m		0.0031	
Rate per Second at 117 m	0.011	0.0035	0.0030
Rate per Second at 238 m		0.0032	0.0024
Rate per Second at 366 m	0.015	0.0036	0.0028
Rate per Second at 719 m	0.014	0.0039	0.0036
Rate per Second at 921 m			0.0032
Rate per Second at 1194 m	0.018	0.0042	0.0038

Table 4.7: SEU Rate Per Second Per Centimetre Squared at Different Elevations at ISO 6400

Camera	Canon T2i	Canon 5D Mark II	Canon 5DSR
Sensor Size [cm x cm]	2.23 x 1.49	3.6 x 2.4	3.6 x 2.4
Rate per Second at 5 m	0.045	0.0065	0.0066
Rate per Second at 77 m		0.0073	
Rate per Second at 117 m	0.033	0.0066	0.0066
Rate per Second at 238 m		0.0065	0.0063
Rate per Second at 366 m	0.14	0.0065	0.0066
Rate per Second at 719 m		0.0079	0.0080
Rate per Second at 921 m			0.0074
Rate per Second at 1194 m	0.23	0.0091	0.0088

Table 4.8: SEU Rate Per Second Per Centimetre Squared at Different Elevations at ISO 12800

Camera	Canon 5D Mark II	Canon 5DSR
Sensor Size [cm x cm]	3.6 x 2.4	3.6 x 2.4
Rate per Second at 5 m	0.012	0.012
Rate per Second at 77 m	0.013	
Rate per Second at 117 m	0.011	0.012
Rate per Second at 238 m	0.011	0.014
Rate per Second at 366 m	0.012	
Rate per Second at 719 m	0.015	0.014
Rate per Second at 921 m		0.013
Rate per Second at 1194 m	0.014	0.056

From Table 4.5 through Table 4.8, it is apparent that the Canon T2i has the highest rates of SEUs per second per centimetre squared, while the Canon 5DSR generally has the second highest rate followed by the Canon 5D Mark II. Interestingly, as ISO increases, the rates for the Canon 5DSR and 5D Mark II are much closer to each other, with the rates in Table 4.8 being very close for the two columns.

4.6. SEU Charge Distribution

The MATLAB script used to locate SEUs also calculates the charge of each SEU pixel or cluster, from the pixel intensity. Using the charges from a collection of SEUs, a histogram of the charge distribution can be produced. These charge distribution histograms can be produced for each combination of camera, ISO, and elevation, meaning in total there are over 70 different combinations, so each individual charge distribution will not be shown in this thesis. However, the shape of nearly all the histograms is roughly the same. For comparison's sake, each histogram will be plotted with bins of the same size, where the bins have a width of 8192, or 2^{13}, and begin at zero. Note that out of all the histograms, none have any SEUs with charges that belong in the first bin, as the lowest charge is always greater than 8192 from this data. An example of the general shape of these histograms is shown in Figure 4.13.
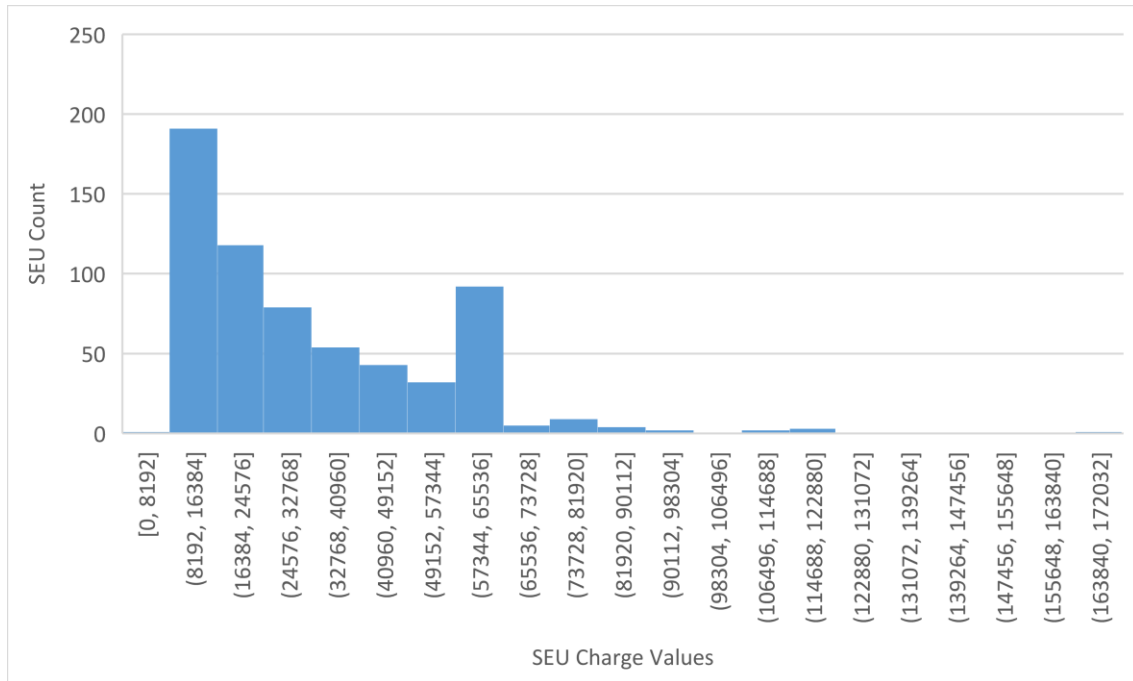

Figure 4.13: Charge Distribution Histogram for the Canon 5DSR at ISO 3200 and an Elevation of 238 metres

From Figure 4.13, one can see that there are two discernable peaks, one in the second bin (the bin beginning at 8192), and a second, smaller peak in the 8th bin (the bin beginning at 57344). The histograms for nearly all combinations of camera, ISO, and elevation follow this exact pattern, where there is a first, larger peak in the second bin, and a smaller, second peak in the 8th bin, with almost no exceptions. The exact same pattern was also noted in previous research [12], [13].

To find patterns in the data, the following figures show a sample of what the different histograms look like for different elevations. Figure 4.14 through Figure 4.20 are the charge distributions from the Canon 5DSR, all at ISO 3200, and in order of increasing elevation. A mid-range ISO was used to give a good example of what a normal collection of charge distributions look like, since at high ISOs the charge distributions tend to look a little different, which will be discussed in more detail later.

Figure 4.14: Charge Distribution Histogram for the Canon 5DSR at ISO 3200 and an Elevation of 5 metres

Figure 4.15: Charge Distribution Histogram for the Canon 5DSR at ISO 3200 and an Elevation of 117 metres

Figure 4.16: Charge Distribution Histogram for the Canon 5DSR at ISO 3200 and an Elevation of 238 metres

Figure 4.17: Charge Distribution Histogram for the Canon 5DSR at ISO 3200 and an Elevation of 366 metres

Figure 4.18: Charge Distribution Histogram for the Canon 5DSR at ISO 3200 and an Elevation of 719 metres[1]

---

[1] For the data at 719 metres, only 366 photos were taken, rather than the usual 1000
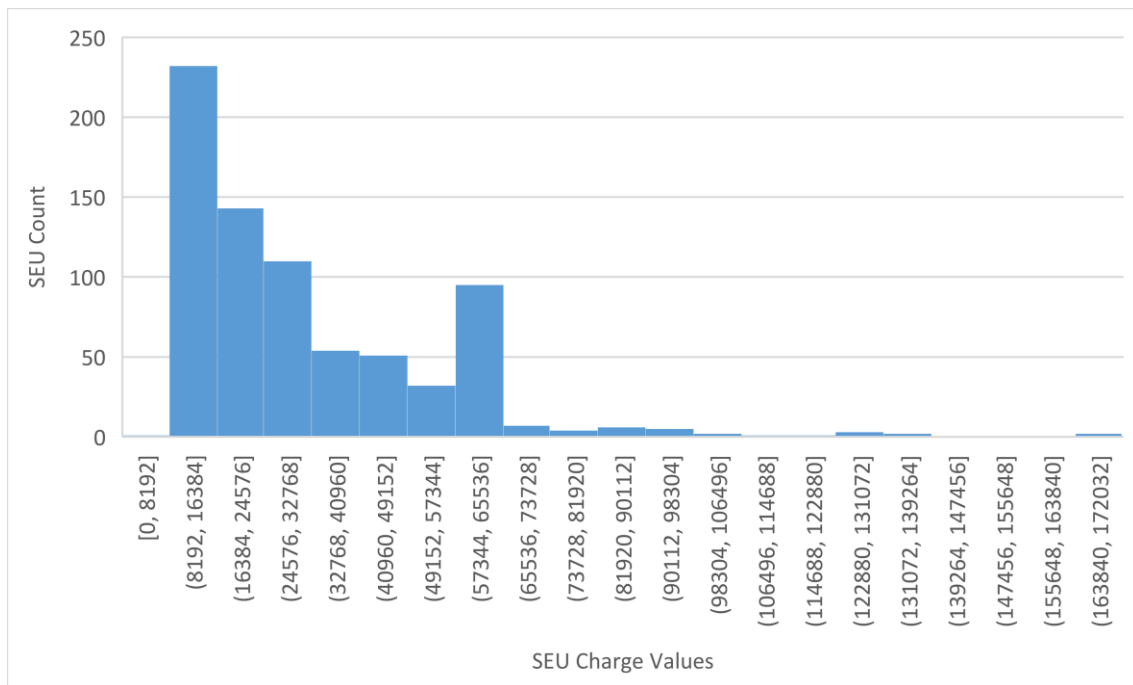
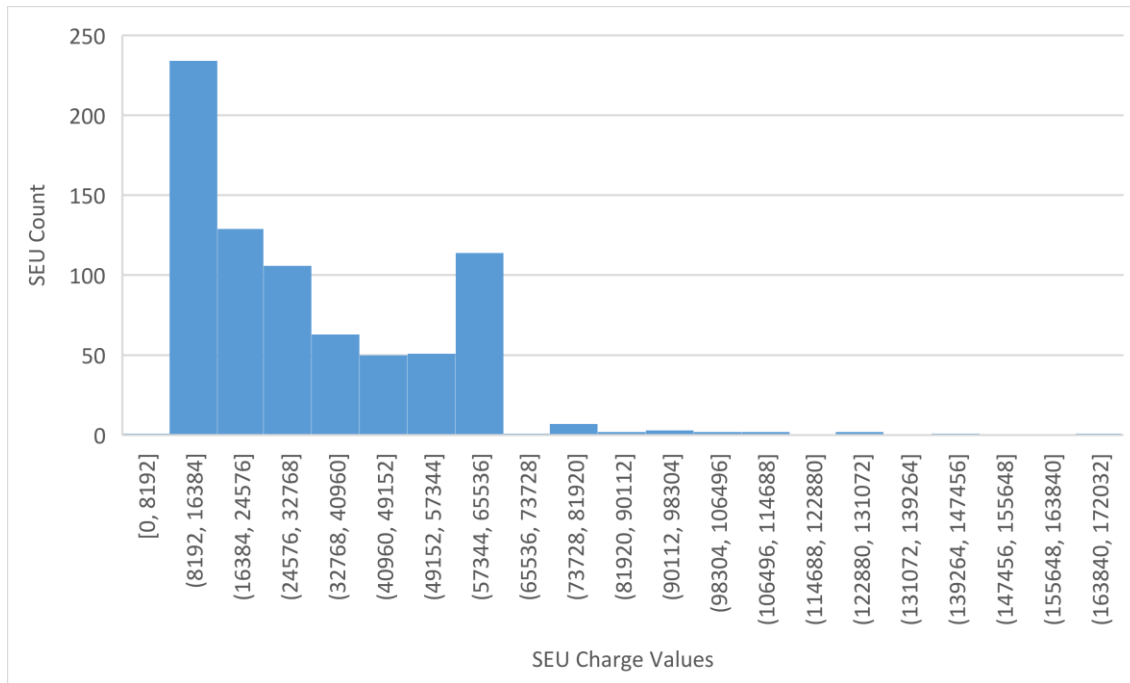*Figure 4.19: Charge Distribution Histogram for the Canon 5DSR at ISO 3200 and an Elevation of 921 metres[2]*

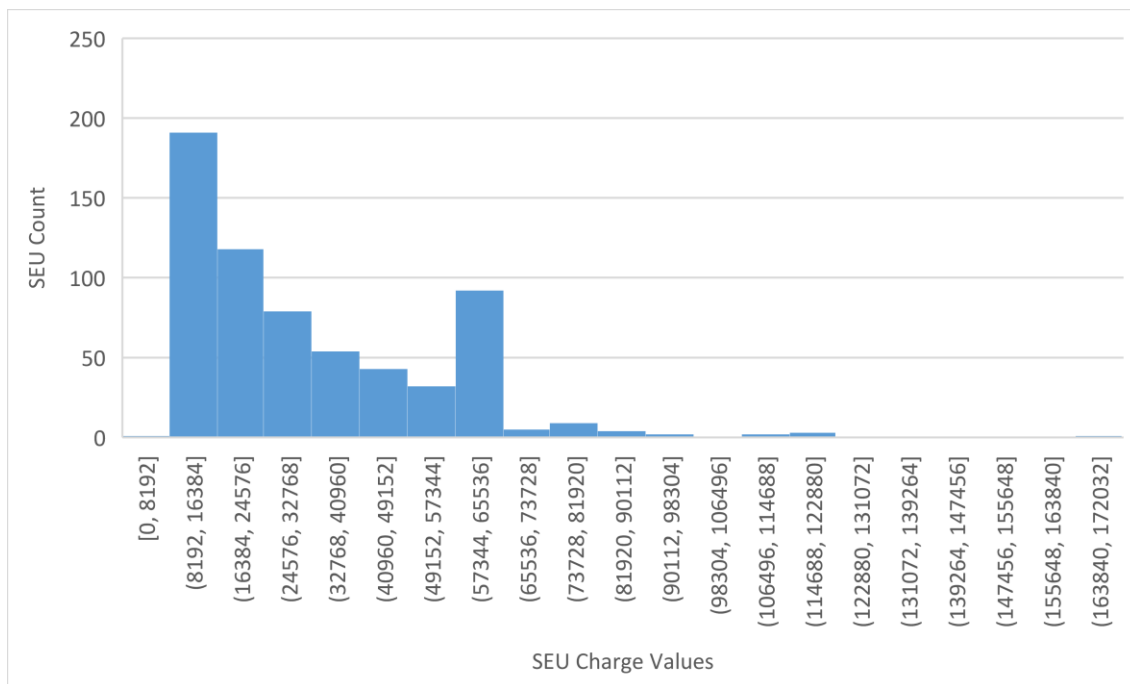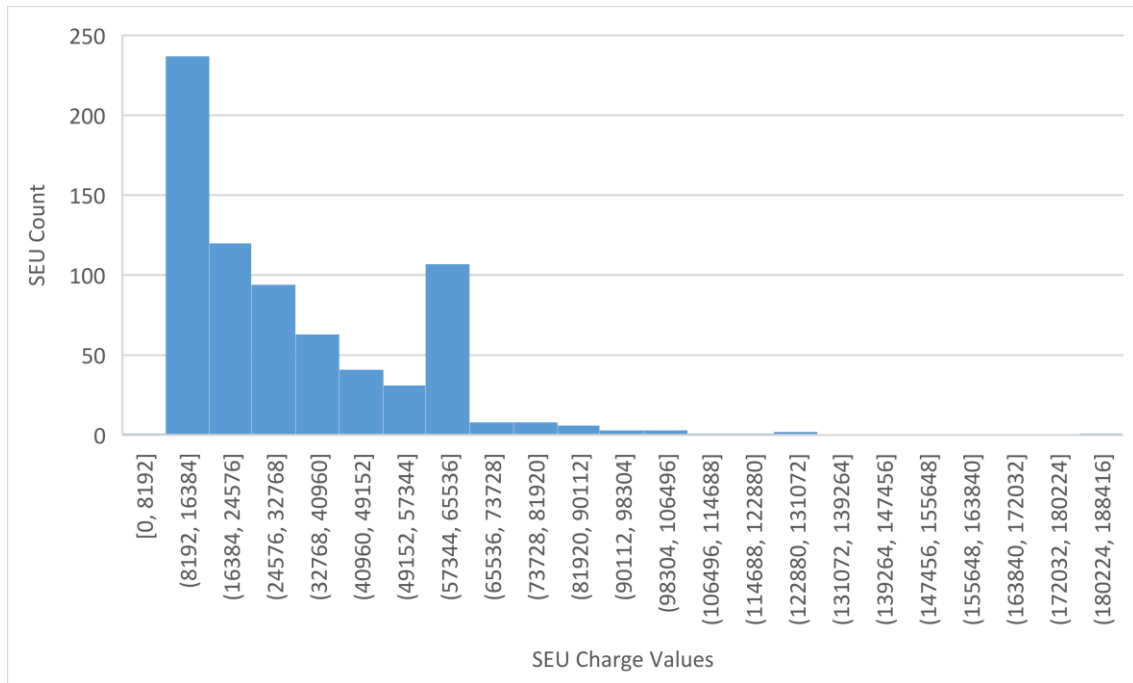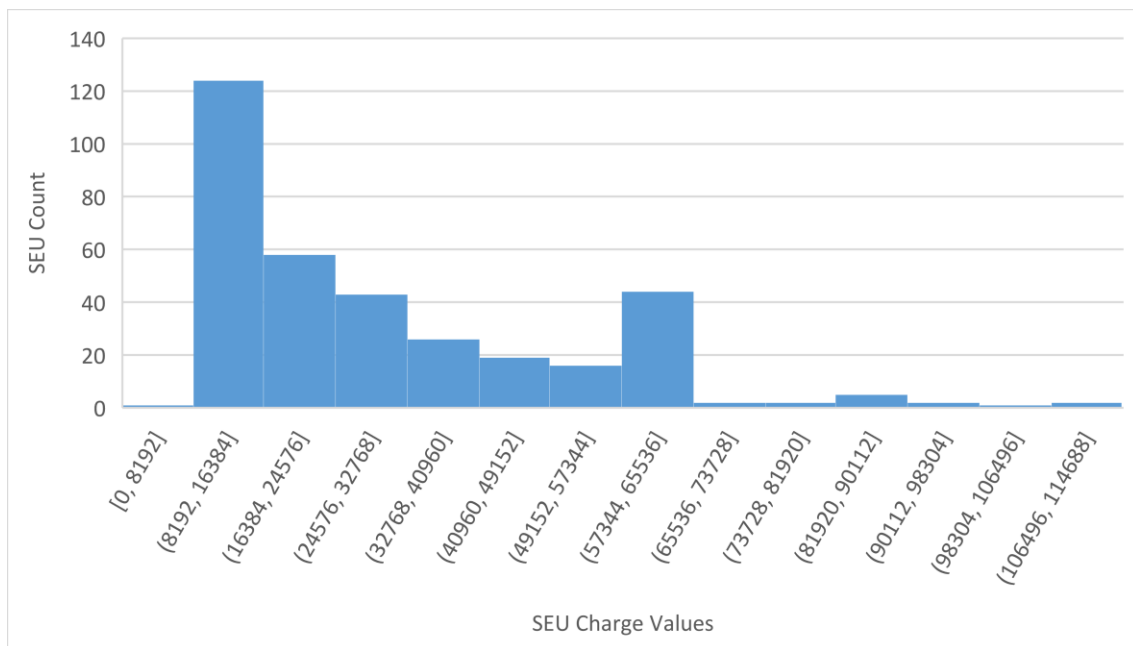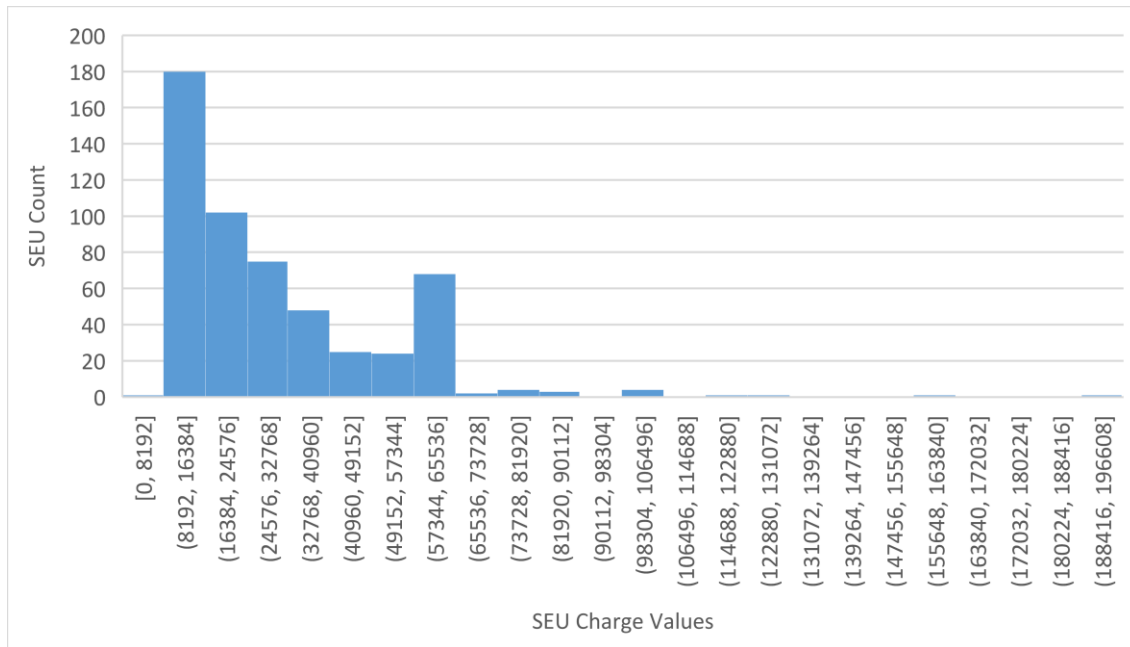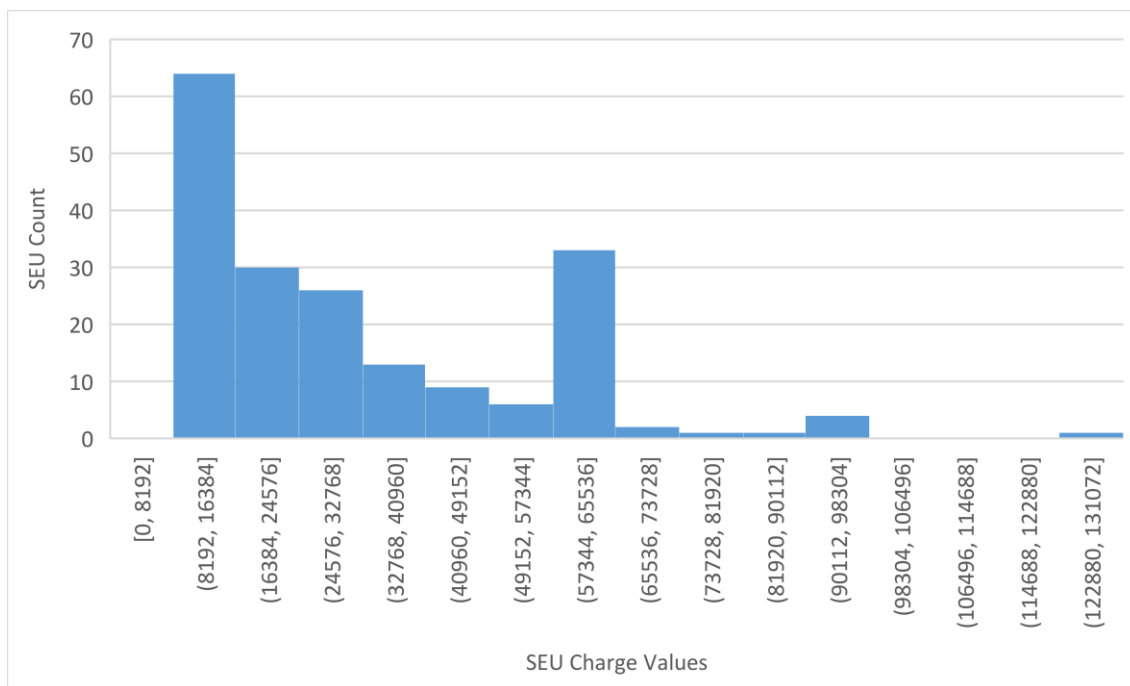*Figure 4.20: Charge Distribution Histogram for the Canon 5DSR at ISO 3200 and an Elevation of 1194 metres[3]*

---

[2] For the data at 921 metres, only 638 photos were taken, rather than the usual 1000

[3] For the data at 1194 metres, only 190 photos were taken, rather than the usual 1000

In Figure 4.14 through Figure 4.20, there is a large peak in the second bin and a smaller peak in the 8th bin, as previously mentioned. As before, the data is skewed to the right, with the bulk of the data points towards the left of the plot and a very long tail. Previous research [12], [13] mentions that as the elevation increases, the tail shortens. Looking at Figure 4.14 through Figure 4.20, it can be hard qualitatively to determine whether the tail is shortening. Rather, a numerical approach will be used where the "skewness" is calculated. Skewness, denoted by $\widetilde{\mu_3}$, returns a number where the sign denotes whether it is left or right skewed (with positive being right skewed, and vice versa), and the magnitude corresponds to the degree of skewness. To calculate skewness Equation (4.3) below is used, where X is the value of each sample, μ is the mean, σ is the standard deviation, and $E[x]$ denotes the expected value of a variable x [31].

$$\widetilde{\mu_3} = E\left[\left(\frac{X - \mu}{\sigma}\right)^3\right]$$

(4.3)

Table 4.9 below lists the skewness, calculated from Equation (4.3), for the histograms from Figure 4.14 to Figure 4.20. The hypothesis, based on previous data, is that as elevation increases, the tail of the charge distribution histogram will become shorter, corresponding to a decrease in skewness.

Table 4.9: Elevation vs. Skewness for the Canon 5DSR at ISO 3200

Elevation	Skewness
5 m	1.79
117 m	1.33
238 m	1.27
366 m	1.20
719 m	1.18
921 m	2.04
1194 m	1.17

From Table 4.9, this research confirms the assumption from previous data. The only exception that should be noted is in the second to last row of the table, the skewness at 921 metres dramatically increases, before falling back down to the expected value. A possible cause for this discrepancy could be that for the elevations 719 metres, 921 metres, and 1194 metres, fewer than 1000 photos were taken. However, at 921 metres, 638 photos were taken, which should still be enough to give a reasonable value for the skewness, also considering that far fewer photos were taken at 719 metres and 1194 metres, but these elevations still have reasonable values for skewness.

Another possible cause of the drastic increase in skewness could be any extreme outliers. From the histogram in Figure 4.19 it is difficult to notice any outliers due to the scale of the y-axis, so instead, the same distribution is plotted on a boxplot in Figure 4.21 below.
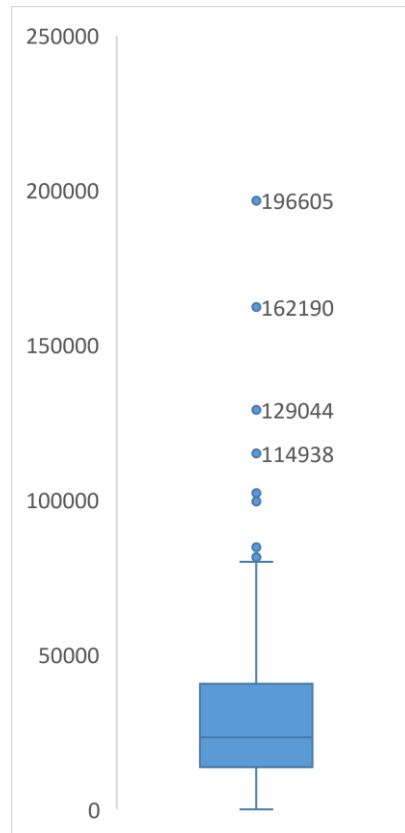

Figure 4.21: Boxplot of the Charge Distribution of SEUs from the Canon 5DSR at ISO 3200 and an Elevation of 921 metres

From the box plot, it is apparent there are multiple outliers, with the largest four being labeled. If the largest outlier, at 196605 is removed, the skewness falls from 2.04 to 1.56, and if the two largest outliers are removed the skewness drops further to 1.29. From Table 4.9, we would expect a skewness of approximately 1.17, but 1.29 is clearly closer to the expected value than 2.04. Since it is generally bad practice to simply remove outliers, they will be kept, but simply knowing that these outliers in the charge distribution at 921 metres are affecting the skewness considerably gives a better understanding of why there is such a huge jump in skewness from 719 metres to 921 metres and then going back down from 921 metres to 1194 metres.

Now that we have confirmed that the tail of the charge distribution histograms shortens as elevation increases, we should discuss what this means. A lower value for skewness would correspond to more data in the leftmost bins, meaning more of the SEUs detected have lower energies. This means at higher elevations, more low energy SEUs are detected compared to the amount of high energy SEUs, which is exactly what was predicted in section 4.4.

Next, as ISO changes, one would possibly expect both peaks of the charge distribution histograms to increase by the same factor, or perhaps one of the two peaks would increase relative to the other depending on if more weak SEUs or strong SEUs are visible at higher ISOs. To determine the relationship between ISO and the charge distribution, histograms from all three cameras were looked at, but to demonstrate, the histograms from the Canon 5D Mark II will be discussed mainly. The reason for choosing the 5D Mark II is that it includes four ISOs, while the T2i only includes three, and for the 5DSR the data includes the highest ISO, which becomes extremely noisy. The effect of noise on the charge distribution histograms at high ISOs will be briefly discussed later. Figure 4.22 to Figure 4.25 show the charge distribution from the Canon 5D Mark II all at the same elevation, but with increasing ISO.

Figure 4.22: Charge Distribution Histogram for the Canon 5D Mark II at ISO 1600 and an Elevation of 77 metres

Figure 4.23: Charge Distribution Histogram for the Canon 5D Mark II at ISO 3200 and an Elevation of 77 metres

Figure 4.24: Charge Distribution Histogram for the Canon 5D Mark II at ISO 6400 and an Elevation of 77 metres
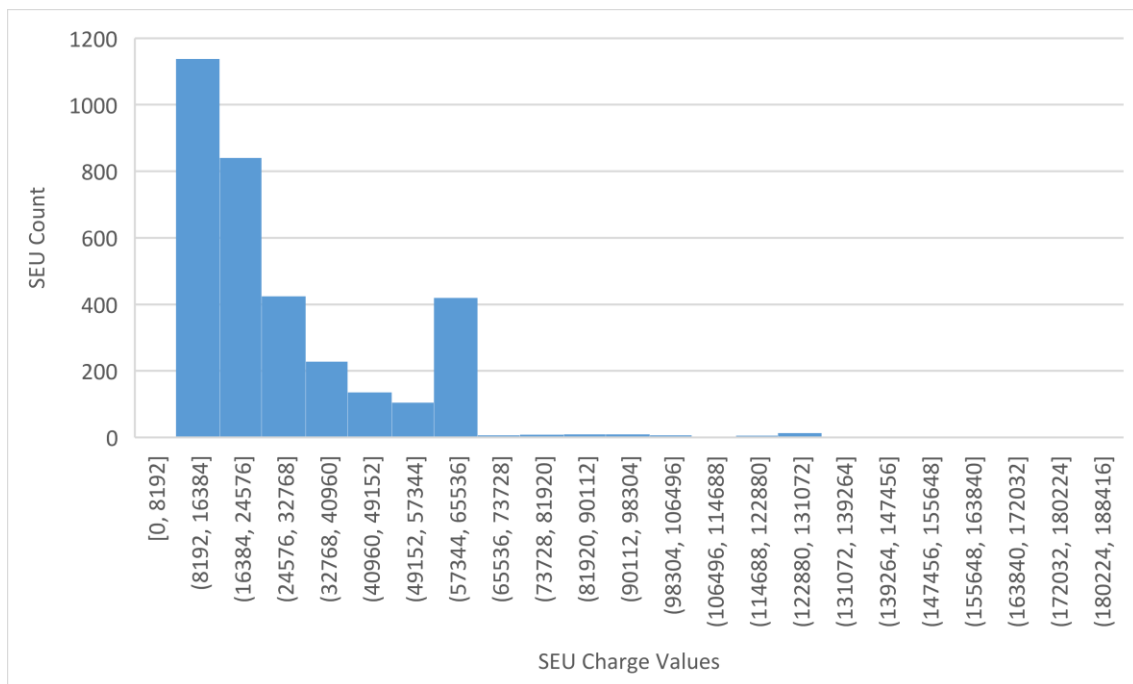
Figure 4.25: Charge Distribution Histogram for the Canon 5D Mark II at ISO 12800 and an Elevation of 77 metres

From Figure 4.22 through Figure 4.25 it is clear that as ISO increases, the height of both peaks increases, however the second peak increases more compared to the first. This essentially means that at higher ISOs more SEUs are detected overall, but especially strong SEUs. Additionally, at higher ISOs the data is more skewed to the right, with a longer tail which also represents stronger SEUs being detected.

The Canon 5DSR has a similar pattern to the Canon 5D Mark II as ISO increases, where both peaks increase, with the second peak increasing by a larger factor than the first peak. However, the Canon T2i exhibits different behaviour. If you look at only ISO 1600 and 3200 for the Canon T2i, the same pattern holds, however the change occurs when you compare ISO 3200 to ISO 6400, shown in Figure 4.26 and Figure 4.27.
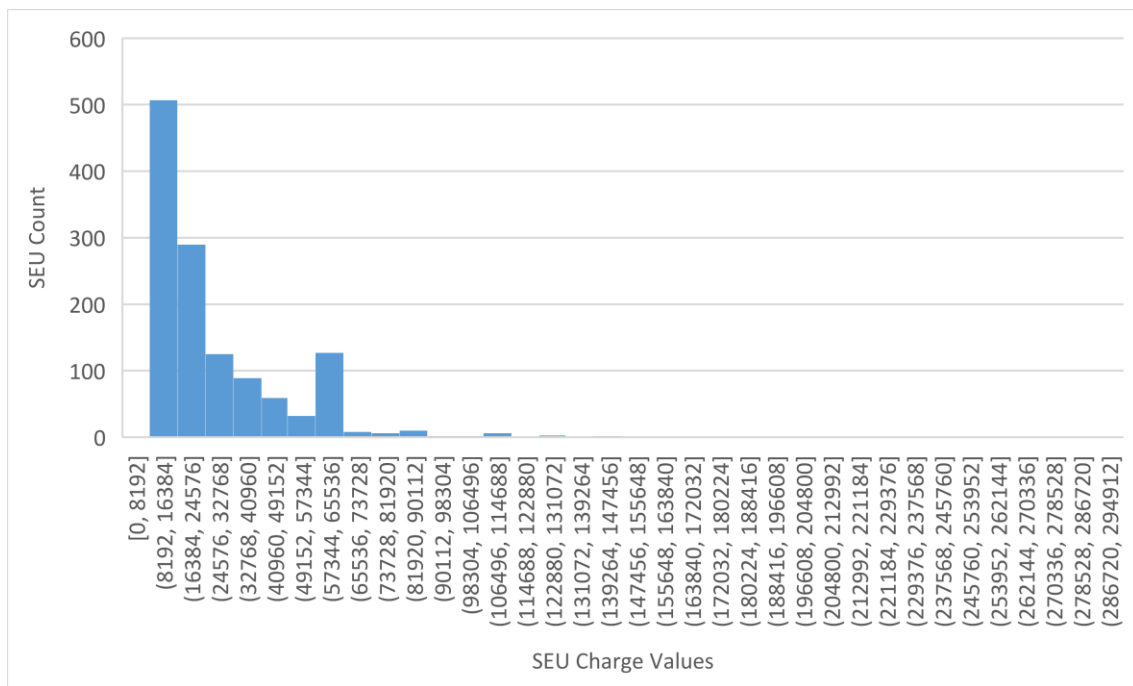
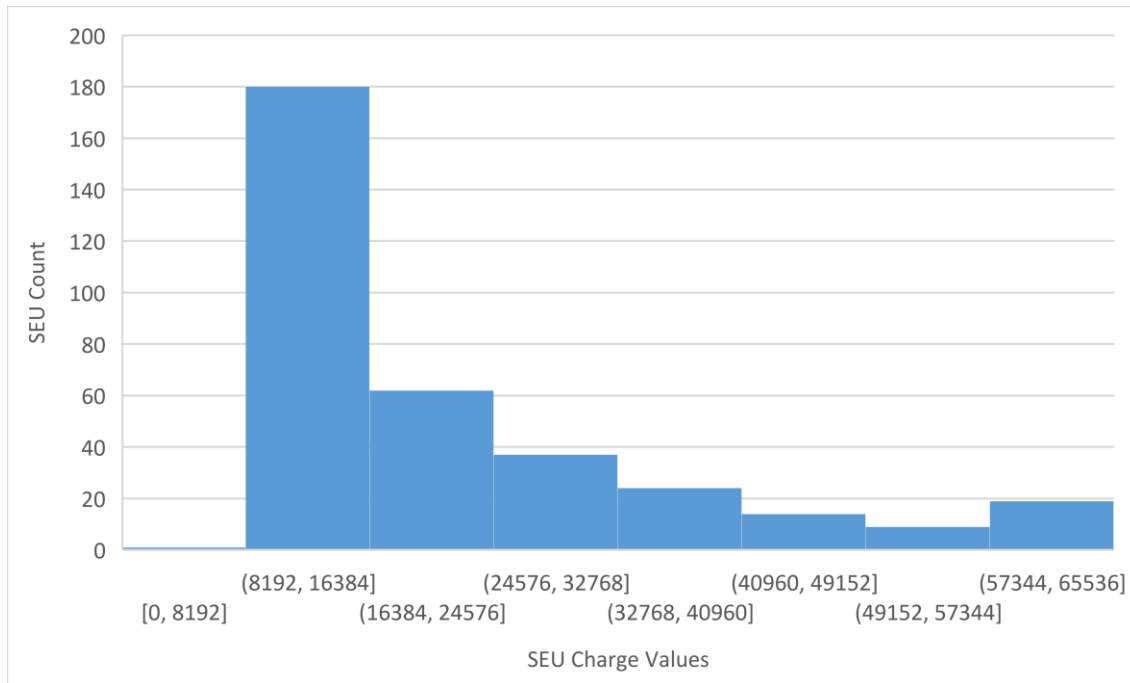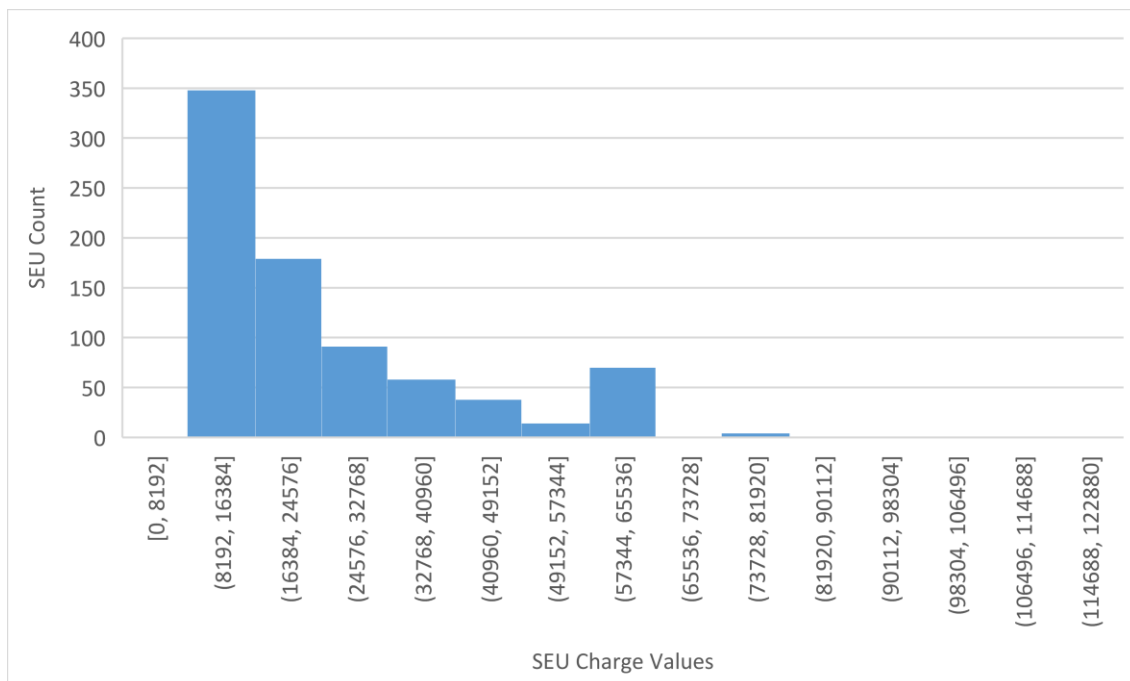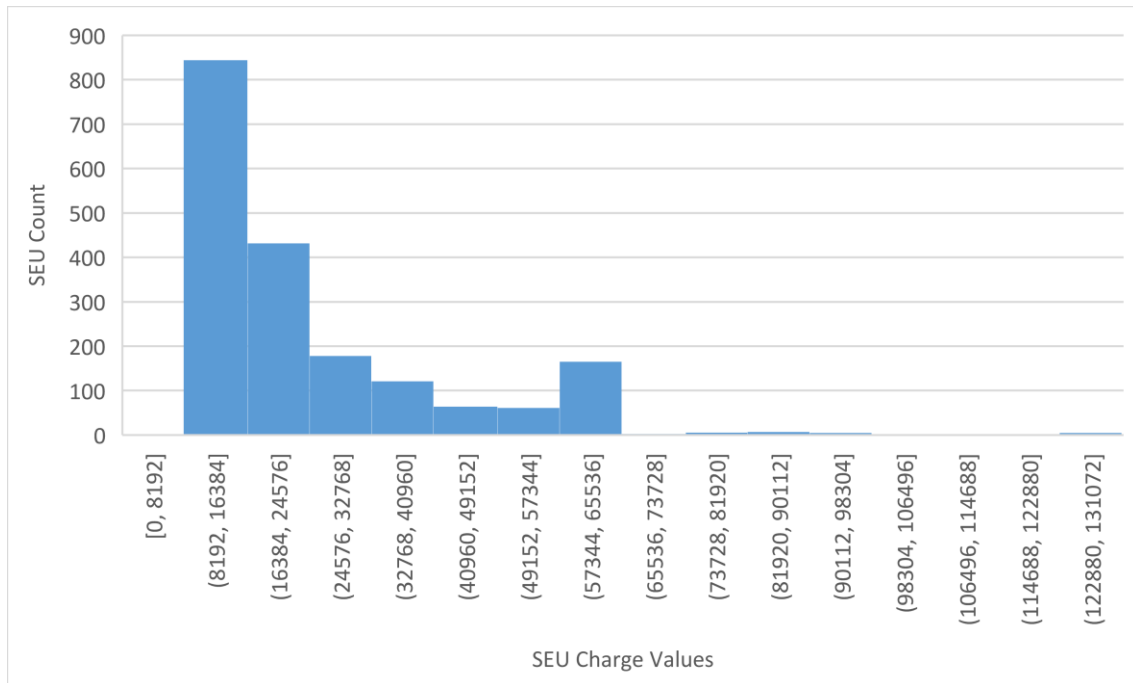*Figure 4.26: Charge Distribution Histogram for the Canon T2i at ISO 3200 and an Elevation of 5 metres*
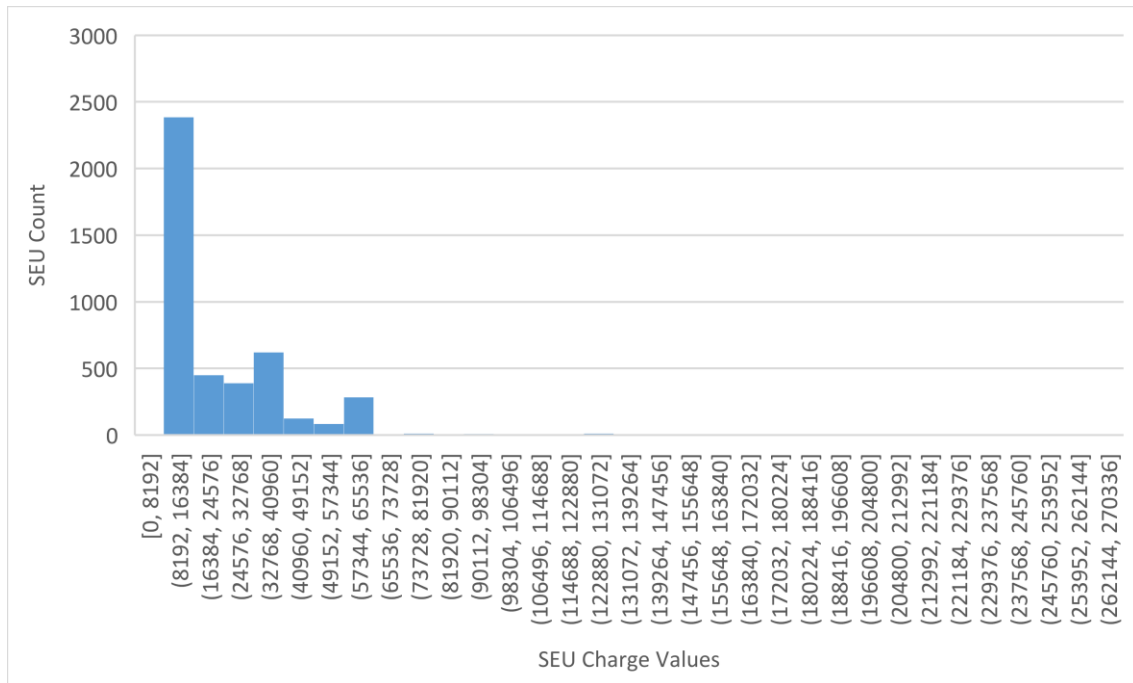
Figure 4.27: Charge Distribution Histogram for the Canon T2i at ISO 6400 and an Elevation of 5 metres

At ISO 6400 for the Canon T2i, in Figure 4.27, there are three peaks instead of two. The first peak is at the same place, still in the second bin, however there is a new second peak in the fifth bin, and there is still a final peak in the eighth bin, however the final peak does not increase by a factor greater than the first peak such as before. Out of all the charge histograms, the ones from the Canon T2i at ISO 6400 (at all elevations) are the only ones with these characteristics. A probable explanation for it is that ISO 6400 is the highest ISO the Canon T2i can be set to. For photography with the Canon T2i, it's only reasonable to use it up to ISO 1600 or possibly 3200 since ISO 6400 becomes very noisy. Another thing to notice is the magnitude of the first peak, in Figure 4.27 it is about five times as high as it is in Figure 4.26. In comparison, for other cameras and combinations of ISOs, when the ISO is doubled, the magnitude of the first peak also doubles, approximately. Likely, this is also due to increased noise at high ISOs, since the Canon 5DSR also showed a huge increase in low charge SEUs at ISO 12800 and 1194 metres in elevation. Due to these issues at high ISOs, for any future research I would suggest avoiding testing at the highest ISO available on a given camera. Possibly research could be put into creating an even more reliable algorithm to separate the noise from the SEUs

53

to make testing at very high ISOs possible. However, there is always going to be a point when the noise will saturate the image and detecting SEUs becomes impossible.

4.7. Unexpected Results

One unanticipated finding was discovered early on when first selecting locations to preform the tests at. All locations had to be relatively easy to travel to, have power available so the cameras can be plugged in, and be somewhere the tests could be run for extended periods of time without interruption, or at the very least with minimal interruptions. For many elevations this was easy, the tests could be performed in people's homes or at SFU, however for higher elevations it was more difficult to find suitable locations. Now, for the "sea level" elevation, which ended up being 5 metres above sea level, the original location chosen was different. Originally, the location chosen was in the town of Harrison Hot Springs and had an elevation of 14 metres. The sea level tests were begun there, but then moved to Agassiz, about 8 kilometres South of Harrison Hot Springs. The two spots had nearly identical elevations and latitudes, so based on all our previous research there should not be a significant difference in SEU levels at the two locations. However, we found extremely high levels of defects at Harrison Hot Springs, and high levels in Agassiz, however much less extreme than near the hot springs. From the photos taken in the town of Harrison Hot Springs, about 1 kilometre from the source of the hot springs, there were too many defects for our MATLAB script to analyze the 1000 photos in a reasonable amount of time, so instead only 100 photos were analyzed. From those 100 photos there were over 30,000 defects found at ISO 12800 in the Canon 5DSR, which if you compare to the values in Figure 4.11 is 100 times the amount that should be expected at that elevation. Meanwhile, in Agassiz which is about 9 kilometres away from the hot springs, the levels were about 15 times higher than should be expected, which is significantly lower than in Harrison Hot Springs (although still to high to continue running our tests there), meaning the hot springs are likely the source of the additional defects.

The minerals present in Harrison Hot Springs are potash and sulphur [32], both of which can have radioactive isotopes, although the sulphur isotopes that exist in nature are not radioactive [33], [34]. Consequently, radioactivity from potassium isotopes in potash is the likely cause of the increase in defects here. In the future, it would be wise to avoid

collecting data in the vicinity of any hot springs or other known sources of even mild radioactivity. Once the increased defects near the hot springs were discovered, the "sea level" tests were moved to Port Coquitlam, about 50 kilometres away from the hot springs.

4.8. Summary

In this chapter, we began by introducing conclusions made from previous research, then new data was presented and explained. There were three ways the data was presented, first graphs showing the number of SEUs present in 1000 photographs was plotted against elevation, next the rates of SEUs per second per centimetre squared was listed, and last charge distribution histograms of the SEUs for various datasets were shown and discussed. For the most part, our data matched what was expected, however there were some notable deviances.

Chapter 5.

Conclusion

5.1. Summary

Beginning with the history of cameras and how cosmic rays have been studied in the past, this thesis aimed to explore the relationship between elevation and cosmic rays for elevations from sea level to approximately 1,000 metres above sea level. First, film cameras and their influence on how digital cameras work was described to give the reader enough knowledge to understand any terminology in this thesis. Then, what affects cosmic rays, and how they affect traditional ICs was detailed. The process for collecting data and analyzing it to locate SEUs was described, and then the results were presented. Chapter 4 showed that there is a linear relationship between SEU occurrence rates and elevation for moderate elevations, with data from three cameras ranging from 5 metres to 1194 metres above sea level. It was shown that as elevation increases, so does the frequency of SEUs in digital cameras, and generally, at higher ISOs more SEUs were detected. These results were also compared to neutron flux theory, which also happens to show a linear relationship for elevations less than approximately 20,000 metres above sea level. From the number of SEUs in a set of images, the occurrence rate, which was events per time per area, was calculated. The charge distribution for the SEUs from a set of images was also found and had a very similar pattern that persisted through nearly every combination of ISO and elevation. The charge distribution allows us to determine if the SEUs being detected are strong or weak SEUs, and it was found that the higher the ISO, the higher the ratio of strong to weak SEUs was. For varying elevations, it was difficult to qualitatively determine whether there were more strong or weak SEUs between two elevations, since different elevations had different sample sizes, so instead a quantitative approach was used where the skewness was calculated for each distribution. The results from this showed as elevation rose, the ratio of strong to weak SEUs decreased.

5.2. Future Research

While this thesis added on to prior research [12], [13] on how elevation affects SEU occurrence rates by including more cameras and a much larger range of elevations, there are still many options for other ways to expand this research in the future. Firstly, a wider range of altitudes would be beneficial as this thesis was limited to elevations below 1200 metres. In Vancouver, BC and the surrounding areas we are lucky to have a large range of elevations, however it can be difficult to access elevations higher than 1000 metres, especially for extended periods of time, with the only readily available way being conducting the experiments at ski resorts. For future research it would be advisable to locate ski resorts at elevations higher than 1200 metres, possibly traveling further from Vancouver. However, if a wider range of locations was included, researchers may need to account for how SEU occurrence rates vary with latitude, as mentioned in sections 1.2 and 3.2.3. Additionally, data could be taken during an airplane flight, however this would introduce many more factors to consider. Firstly, the cruising altitude of a plane slightly varies during the duration of a flight, luckily most modern commercial planes display the current altitude of the plane during the flight, so the average cruising altitude could be recorded. Secondly, the latitude will change significantly during most flights, meaning if you are taking hundreds of photos, the latitude could vary greatly from the first to the last photo, which will inherently cause the SEU rates to change.

Another aspect which would be studied more in the future is including additional cameras, as only three DSLRs were used here. In the future other types of digital cameras such as mirrorless, or cell phone cameras could be used at varying elevations. Some difficulties with this are that the camera must be able to output photographs in RAW format and must be compatible with some type of intervalometer to record the pictures. Currently, many mirrorless cameras, while they do support RAW format, are not compatible with the intervalometer software used here, such as Magic Lantern, Canon EOS Utility, and Astro Photography Tool. With regards to cell phone cameras, it would be interesting to see how significantly smaller pixel sizes affect SEUs. Since cameras are only beginning to support RAW format, third-party apps may need to be used to shoot in RAW for many phones, but it is becoming more viable to expand this research to include cell phones at different elevations. However, in addition to needing an intervalometer and being able to shoot in

RAW, there is the issue of a huge increase in noise with cellphone cameras, meaning the ISOs used must be much lower than they were in this thesis.

Lastly, an area of concern in this thesis was how reliable our detection methods are at extremely high ISOs. As previously mentioned, when using the highest ISO available in each camera the amounts of SEUs seemed to deviate from the expected values more than at lower ISOs. Possibly, in the future more reliable detection algorithms could be developed. However, this would come with a trade-off of processing time, as the current algorithm already takes hours to compute the number of SEUs. Additionally, it is likely that a maximum for how much noise can be tolerated is surpassed at the highest ISO in each camera. Once noise saturates the image, it will be impossible to separate noise from any SEUs, so it is completely possible that even with better detection algorithms it will not be possible to detect SEUs at such high ISOs. If research must be done at the highest ISO on a given camera, a possible way to mitigate the noise would be to decrease the exposure time, however then the SEU rate per second should be used if these photos are compared to any with a different exposure time.

5.3. Closing Remarks

After analyzing data from multiple DSLR cameras at elevations ranging from sea level to 1200 metres we have been able to determine the linear relationship between elevation and SEU rates for modest elevations. This can be compared to the relationship between neutron flux and elevation at similar elevations, which also exhibits linear behaviour. The charge distributions of SEUs from these datasets were also analyzed to determine when digital imagers are more sensitive to weak SEUs or strong SEUs, with high elevations resulting in more weak SEUs being detected and high ISOs resulting in more strong SEUs being detected.

References

[1]   T. Gustavson, *Camera: A History of Photography from Daguerreotype to Digital*. Sterling Innovation, 2009.

[2]   G. C. Holst, *CMOS/CCD sensors and camera systems / Gerald C. Holst, Terrence S. Lomheim.*, 2nd ed. JCD Publishing ; SPIE, 2011.

[3]   M. Bertolotti, *Celestial Messengers: Cosmic Rays*. Springer, 2012.

[4]   S. Biswas, *Cosmic Perspectives in Space Physics*, 1st ed. 2000. Springer Netherlands : Imprint: Springer, 2000.

[5]   J. F. Ziegler, "Terrestrial Cosmic Rays," *IBM journal of research and development*, vol. 40, no. 1, pp. 19–39, 1996, doi: 10.1147/rd.401.0019.

[6]   G. Hubert, A. Cheminet, T. Nuns, and V. Lacoste, "Atmospheric Radiation Environment Analyses Based-on CCD Camera, Neutron Spectrometer and Multi-Physics Modeling," *IEEE transactions on nuclear science*, vol. 60, no. 6, pp. 4660–4667, 2013, doi: 10.1109/TNS.2013.2282219.

[7]   J. T. Wallmark and S. M. Marcus, "Minimum Size and Maximum Packing Density of Nonredundant Semiconductor Devices," *Proceedings of the IRE*, vol. 50, no. 3, pp. 286–298, 1962, doi: 10.1109/JRPROC.1962.288321.

[8]   A. Hanslmeier, "The Chaotic Solar Cycle," 2020. [Online]. Available: http://www.springer.com/series/16015

[9]   A. Kaase, "Earth's Magnetosphere," *NASA*, Aug. 07, 2017.

[10]   E. Petersen, *Single Event Effects in Aerospace*. Hoboken, NJ, USA: John Wiley & Sons, Inc., 2011. doi: 10.1002/9781118084328.

[11]   J.-L. Autran and D. Munteanu, *Soft Errors: From Particles to Circuits*, vol. 39. Baton Rouge: CRC Press, 2015. doi: 10.1201/b18132.

[12] G. H. Chapman, R. Thomas, K. J. Meneses, R. Zhao, I. Koren, and Z. Koren, "Using Digital Imagers to Characterize the Dependence of Energy and Area Distributions of SEUs on Elevation," 2020. doi: 10.1109/DFT50435.2020.9250888.

[13] R. Thomas, "Detection and Analysis of Single Event Upsets in Noisy Digital Imagers with Small to Medium Pixels," 2020.

[14] P. P. Shirvani and E. J. Mccluskey, "SEU Characterization of Digital Circuits Using Weighted Test Programs SEU Characterization of Digital Circuits Using Weighted Test Programs," May 2001.

[15] Z. Torok and S. P. Platt, "Application of Imaging Systems to Characterization of Single-Event Effects in High-Energy Neutron Environments," *IEEE transactions on nuclear science*, vol. 53, no. 6, pp. 3718–3725, 2006, doi: 10.1109/TNS.2006.885005.

[16] A. M. Chugg *et al.*, "Analyses of CCD images of nucleon-silicon interaction events," *IEEE transactions on nuclear science*, vol. 51, no. 5, pp. 2851–2856, 2004, doi: 10.1109/TNS.2004.835113.

[17] P. E. Dodd and L. W. Massengill, "Basic Mechanisms and Modeling of Single-Event Upset in Digital Microelectronics," *IEEE Transactions on Nuclear Science*, vol. 50, no. 3, pp. 583–602, 2003, doi: 10.1109/TNS.2003.813129.

[18] F. Firouzi, M. E. Salehi, F. Wang, and S. M. Fakhraie, "An Accurate Model for Soft Error Rate Estimation Considering Dynamic Voltage and Frequency Scaling Effects," *Microelectronics and reliability*, vol. 51, no. 2, pp. 460–467, 2011, doi: 10.1016/j.microrel.2010.08.016.

[19] B. E. Bayer, "Color Imaging Array." Rochester, NY, Jul. 20, 1976.

[20] G. H. Chapman, "Digital Camera Technology." 2020.

[21] R. Thomas, "Enhanced Digital Imager Defect Analysis with Smaller Pixel Sizes," 2016.

[22] T. J. Jensen, *Budget Astrophotography*. New York, NY: Springer New York, 2014.

[23]   K. Irie, I. M. Woodhead, A. E. McKinnon, and K. Unsworth, "Measured Effects of Temperature on Illumination-Independent Camera Noise," Nov. 2009. doi: 10.1109/IVCNZ.2009.5378403.

[24]   Canon Inc., "Canon EOS 5DSR Instruction Manual." p. 488, Feb. 2017.

[25]   Canon Inc., "Canon EOS 5D Mark II Instruction Manual." p. 234, Jan. 2010.

[26]   Canon Inc., "Canon EOS Rebel T2i Instruction Manual." p. 225, Jan. 2010.

[27]   Distinct Solutions Ltd., "Astro Photography Tool," May 06, 2021. https://www.astrophotography.app/ (accessed Aug. 05, 2021).

[28]   "About Magic Lantern," 2017. https://magiclantern.fm/about.html (accessed Sep. 08, 2021).

[29]   D. C. Montgomery, G. C. Runger, and N. F. Hubele, *Engineering Statistics*, 5th ed. Arizona: Wiley, 2011.

[30]   M. S. Gordon *et al.*, "Measurement of the Flux and Energy Spectrum of Cosmic-Ray Induced Neutrons on the Ground," in *IEEE Transactions on Nuclear Science*, Dec. 2004, vol. 51, no. 6 II. doi: 10.1109/TNS.2004.839134.

[31]   L. Chihara and T. Hesterberg, *Mathematical Statistics with Resampling and R*, 1st edition. Wiley, 2011.

[32]   "Our Hot Springs," *Harrison River Valley*. https://tourismharrison.com/explore/harrison-river-valley/our-region/our-hot-springs/ (accessed Nov. 05, 2021).

[33]   "Fields of Application for Potash," *J & C Bachmann*. https://jcbachmann.com/applications/potash/ (accessed Nov. 05, 2021).

[34]   "Element: Sulphur," *Radiochemistry Society*, 2003. https://www.radiochemistry.org/periodictable/elements/16.html (accessed Nov. 05, 2021).

Appendix A. Calculations to Convert Arcminutes to Kilometres

As latitude is briefly mentioned in this thesis, it is important the audience understands how to interpret the geographic coordinate system. The location of any point on Earth's surface can be defined by latitude and longitude. Latitude ranges from 90° N at the north pole to 90° S at the south pole, while longitude ranges from 180° E to 180° W. When reporting fractions of a degree, either decimals, or arcminutes and arcseconds are used. For example, the coordinates (49.2773275 N ,-122.9143302 W) can also be written as (49°16'38.379" N, 122°54'51.588" W) where ' denotes arcminutes and " denotes arcseconds. One minute of arc corresponds to $\frac{1}{60}$th of a degree and one second of arc corresponds to $\frac{1}{360}$th of a degree.

Converting degrees of latitude to kilometres is a fairly simple calculation, however it gets more complicated if you are converting degrees of longitude to kilometres, since the ratio changes depending on the latitude. Since we are only concerned with degrees of latitude at the moment, only those calculations will be shown. Using Earth's radius of 6371 km, Pythagorean's theorem can be used to get an approximation for how far 20 minutes of arc is.

$$20 \; arcminutes * \frac{1 \; degree}{60 \; arcminutes} = 0.\bar{3} \; degrees$$
$$d = (Earth's \; radius) * \tan(0.\bar{3}°)$$
$$d = 33.36 \; km$$